DESIGN STUDY OF A VUV MICROSCOPE AT 121.6 NM WITH THE SAMPLE IN AIR

by

Derek Keyes

A Thesis Submitted to the Faculty of the

DEPARTMENT OF OPTICAL SCIENCES

In Partial Fulfillment of the Requirements

For the Degree of

MASTER OF SCIENCE

In the Graduate College

THE UNIVERSITY OF ARIZONA

2016

STATEMENT BY AUTHOR

The thesis titled *Design study of a VUV Microscope at 121.6 nm with the Sample in Air* prepared by *Derek Keyes* has been submitted in partial fulfillment of requirements for a master's degree at the University of Arizona and is deposited in the University Library to be made available to borrowers under rules of the Library.

Brief quotations from this thesis are allowable without special permission, provided that an accurate acknowledgement of the source is made. Requests for permission for extended quotation from or reproduction of this manuscript in whole or in part may be granted by the head of the major department or the Dean of the Graduate College when in his or her judgment the proposed use of the material is in the interests of scholarship. In all other instances, however, permission must be obtained from the author.

SIGNED: *Derek Keyes*

APPROVAL BY THESIS DIRECTOR

This thesis has been approved on the date shown below:

Thomas D. Milster
Professor of Optical Sciences

May 6, 2016
Date

Contents

Table of Figures

List of Tables

1. Abstract

The design of a custom VUV microscope is studied. The microscope is designed around a custom high brightness, spectrally narrow VUV source operating at the Hydrogen-Lyman-α (HLA) transition characterized by the emission wavelength of 121.6 nm. The incentive for microscopy at 121.6nm is a transparent window in the air absorption spectrum coinciding with 121.6nm light. This allows for the sample to be in air while the microscope is in an enclosed vacuum or nitrogen environment.

A microscope is built consisting of the VUV source, a low noise, x-ray camera, a custom 120 magnification, 0.3 numerical aperture objective lens, and an assortment of vacuum flanges, nipples, and crosses. The camera is verified to detect the HLA output from the source. The objective lens is capable of achieving an intrinsic resolution of 247 nm with a wavelength of 121.6 nm if the proposed alignment procedure is followed and the fabricated mechanical tolerances are within the specified range.

The objective lens mirrors and the primary mirror cell are fabricated out of specification. Therefore, the best expected optical performance is 0.3 Strehl ratio. In order to improve the optical performance, a few design changes are discussed, including increasing the primary mirror thickness to improve surface figure error and increasing the back thickness of the primary mirror cell in order to reduce the force on the primary mirror from radial adjustment screws.

2. Introduction

The optical design, mechanical design, assembly and initial testing of a VUV microscope is described in this thesis. The microscope is designed to image with a wavelength of 121.6 nm, which is the Hydrogen-Lyman-α transition. The Lyman series is the series of transitions and resulting ultraviolet emission lines of the hydrogen atom as an electron goes from $nq \geq 2$ to $nq = 1$, where nq is the principal quantum number. The transition from $nq = 2$ to $nq = 1$ is called the Lyman-α transition and is characterized by an emission wavelength of 121.6 nm [1].

An issue with wavelengths below about 190 nm is strong absorption by molecular oxygen, which results in air being opaque in the vacuum ultraviolet region of the electromagnetic spectrum. However, there exists a narrow, highly transparent window in the air absorption spectrum precisely at 121.6 nm, as shown in Fig. 1 [1]. For example, a light path of 10 mm in dry air produces roughly 6% absorption of 121.6 nm radiation at 760 torr (1 atm). Additionally, a high vacuum environment (~500mTorr) produces ~2% absorption of 121.6 nm radiation per 1.0 m of path length. The combination of narrow line emission (~4pm), and low absorption in dry air provides an exceptionally useful aspect of HLA radiation [1].

The Hydrogen-Lyman-α microscope provides significant benefits in the area of microscopy, including sub-nanometer feature height resolution of samples collected noninvasively without contacting the sample and high transverse resolution without the need for resolution enhancement techniques. The combination of the mentioned

benefits provides the potential for a four times intrinsic-resolution improvement over current visible optical microscopes that do not require the sample to be in vacuum [2].

The Hydrogen-Lyman-α microscope consists of a custom source supplied by UV Solutions Inc., an Andor Technology x-ray camera, and a custom objective lens all attached to an assortment of vacuum flanges customized to mount optical imaging and illumination components, as shown in Figs. 2 and 3. The microscope operates in a controlled temperature range of 22-22.3^{o}C and pressure range of 100-150 mtorr. In order to minimize the airborne molecular contaminants (AMC), the microscope operates in a class 1000 cleanroom, and the internal vacuum chamber is constantly flushed with high purity nitrogen.

Previous work on imaging in the vacuum ultraviolet (VUV) have been attempted using several methods including Fresnel zone plates, curved mirrors, and complicated sources e.g. synchrotrons and free-electron lasers [3][4][5]. VUV imaging has proven to be a difficult task for most research attempts excluding astronomical imaging, where the optical system and light sources are intrinsically in vacuum [3][4][5]. In this work, the optical system is relatively straightforward, utilizing a custom reflective optical objective, a HLA source, and a commercially available detector.

The HLA microscope is assembled, aligned, and tested at the University of Arizona, College of Optical Sciences. Guidelines for the design, alignment, testing, and integration of the HLA microscope are included in this thesis.

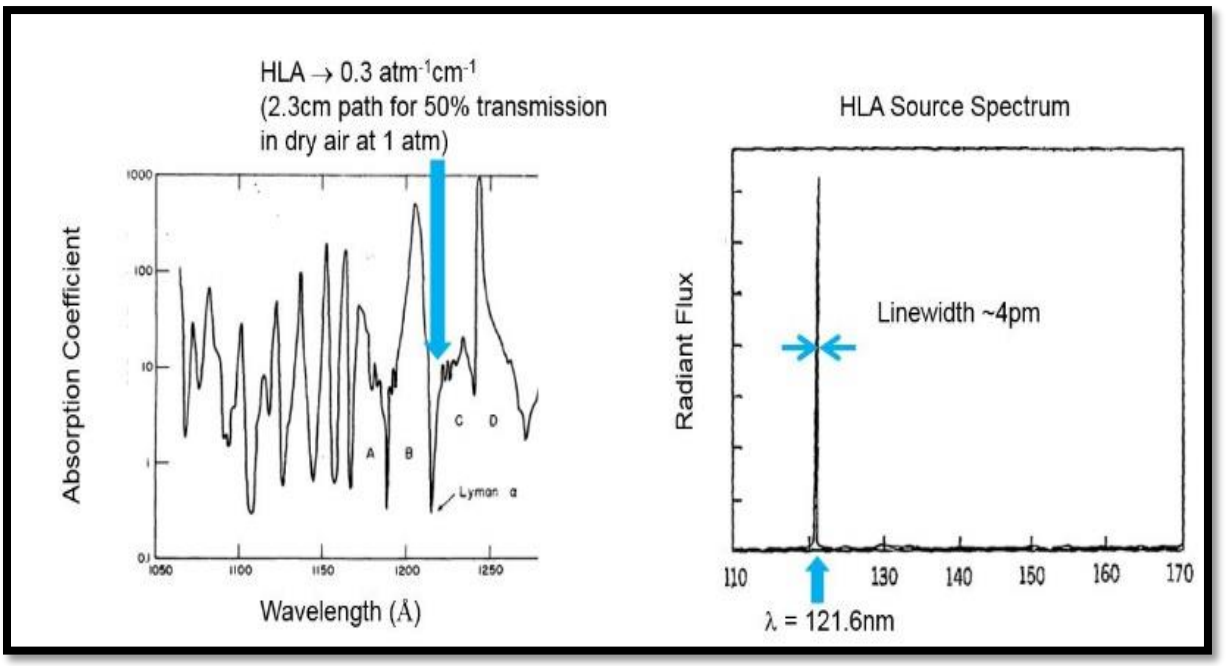

Fig. 1 (Left) Transparent window in air absorption. (Right) HLA Source spectral line width at 121.6 nm

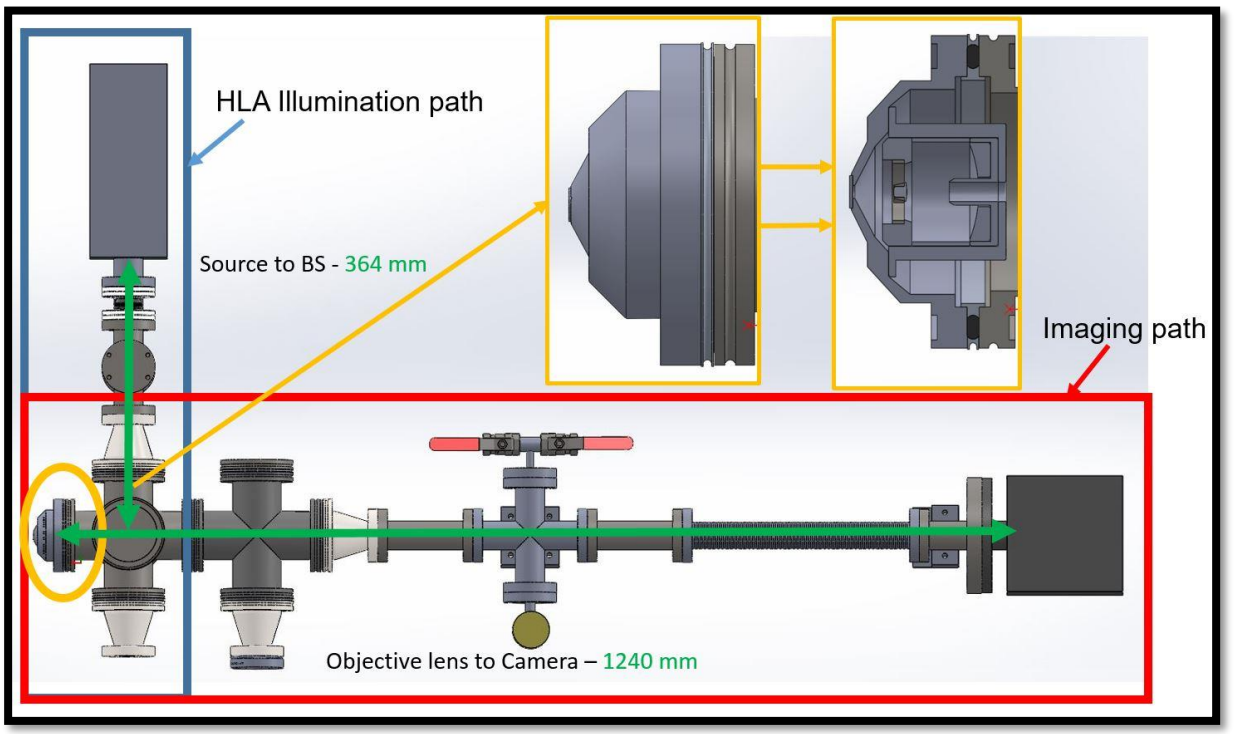

Fig. 2 HLA microscope system model showing the illumination (blue) and imaging paths (red) as well as the location of the objective lens (yellow)

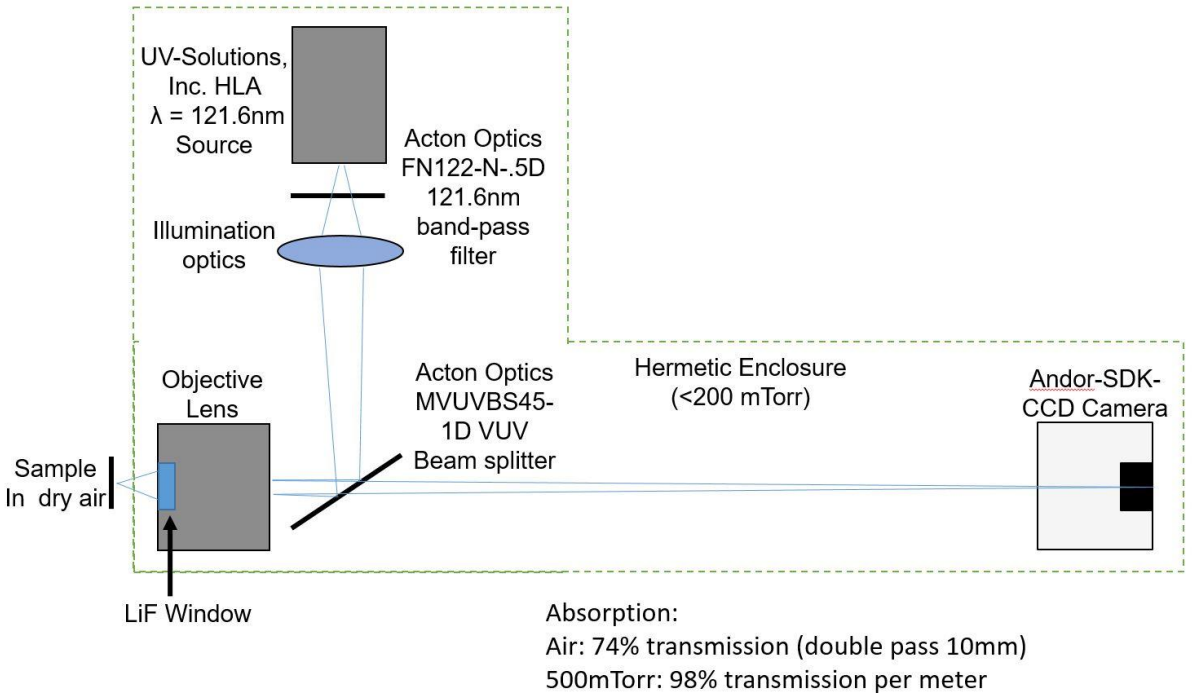

Fig. 3 HLA microscope block diagram

3. HLA Source

The custom 121.6 nm Lyman-Alpha excimer lamp was designed and built by UV Solutions Inc., as shown in Fig.4. The high brightness Lyman-Alpha lamp specifications are listed in Table 1. The output energy is determined by control of the duty cycle via the repetition rate and pulse width. The gas used is research grade neon with approximately 500 ppm of Hydrogen at a pressure between 200 and 500 torr. The chemistry for this process is well described in the paper by McCarthy [3]. The output power of 121.6 nm light reaches a maximum of >10mW/pulse at an operating pressure between 250-300 torr. The pressure of the source is controlled by a gas manifold that allows for a variable flow rate of the gas mixture in and out of the source tube. The tube is 4mm in diameter and contains the radiation region. The 121.6 nm radiation from the tube passes through a MgF2 window in the form of a low divergence beam. A well-shielded 5 MHz RF power supply that produces a maximum power of 15 W is used to power the source. In order to connect the lamp to the microscope vacuum chamber, the lamp housing is fitted with a 2.75” CF flange.

Table 1. HLA Source Specifications

Wavelength	121.6 nm (Lyman Alpha
FWHM	< 0.1 nm
Divergence	~ 3-5 degrees
Beam Area	0.5 mm – 2 mm
Output power	10 mW/pulse
Brightness	10 10mW/mm^2/pulse
Operation	Pulsed, variation with duty cycle
Pulse width	10 µs – 100 µs
Repetition rate	50 Hz – 1000 Hz

.

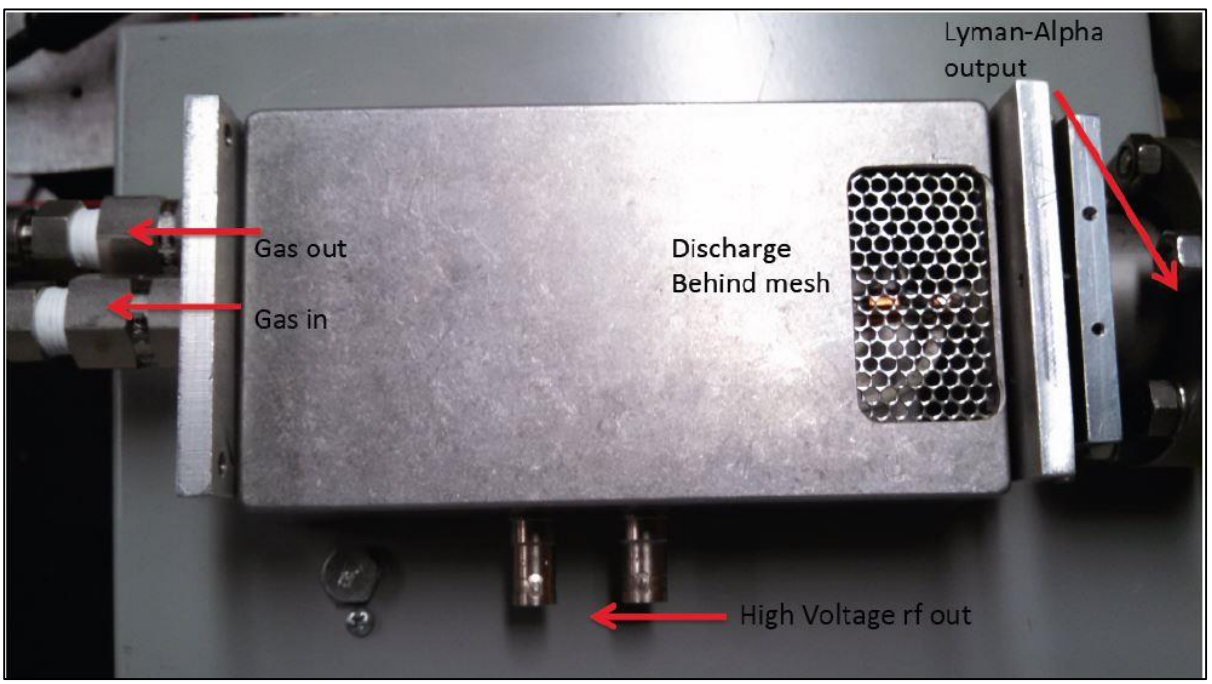

Fig. 4 HLA Lamp

The gas manifold is designed using ¼'' steel tubing, 4 ball-valves, a needle valve, a pressure gauge, an oil-less vacuum pump, and the gas mixture. The basic HLA lamp lighting procedure is listed in Appendix A. The gas in and gas out pressure control valves are Swagelok, lever controlled, stainless steel, ball valves. A common mistake when lighting the source is mistaking high brightness from the mesh grid opening for max HLA wavelength output. As noted above, the maximum 121.6 nm output is at an operating pressure between 250-300 torr. The pump is an Agilent IDP-3 dry, scroll single hermetic vacuum pump with an ultimate pressure of 0.25 Torr. The pressure gauge calibration chart is given in the Appendix A.

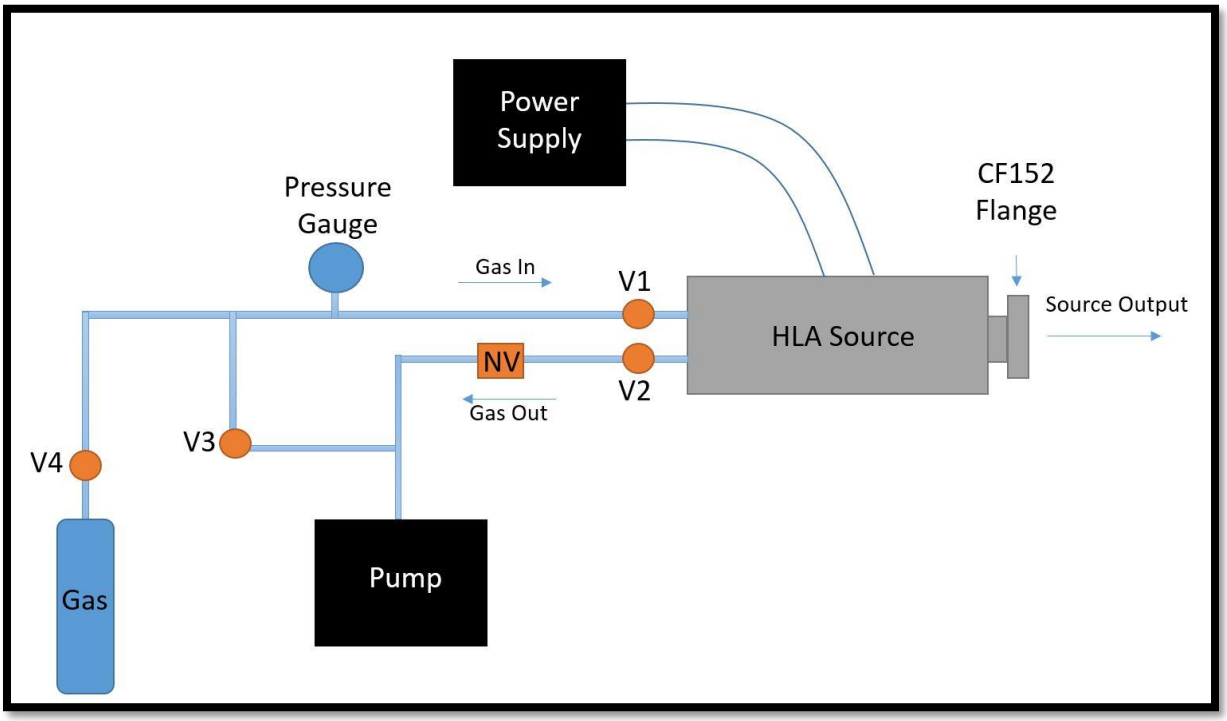

Fig. 5 Schematic of Gas Manifold

4. Camera

The x-ray camera is an Andor iKon-M SO, which is a CCD detector optimized for soft X-ray, EUV, and VUV applications. The specifications of this model are summarized in Table 2. A CF152 flange allows for direct installation to the HLA microscope, as shown in Fig. 5. The sensor is a back illuminated CCD, meaning electrodes are on the bottom surface of the sensor and there is a thin depletion region. This design allows for the detection of soft x-rays, and the quantum efficiency of the sensor is shown in Fig. 4.

Table 2. Camera Specifications

Active pixels	1024 x 1024
Sensor size	13.3 mm x 13.3 mm
Pixel size	13 x 13 μm
Active area pixel well depth	100,000 e^-
Maximum readout rate	5 MHz
Read noise	2.9 e^-
Maximum cooling	-100 °C
Frame rate	4.4 fps (full frame)
Quantum Efficiency (at λ = 121.6 nm)	≈ 4%

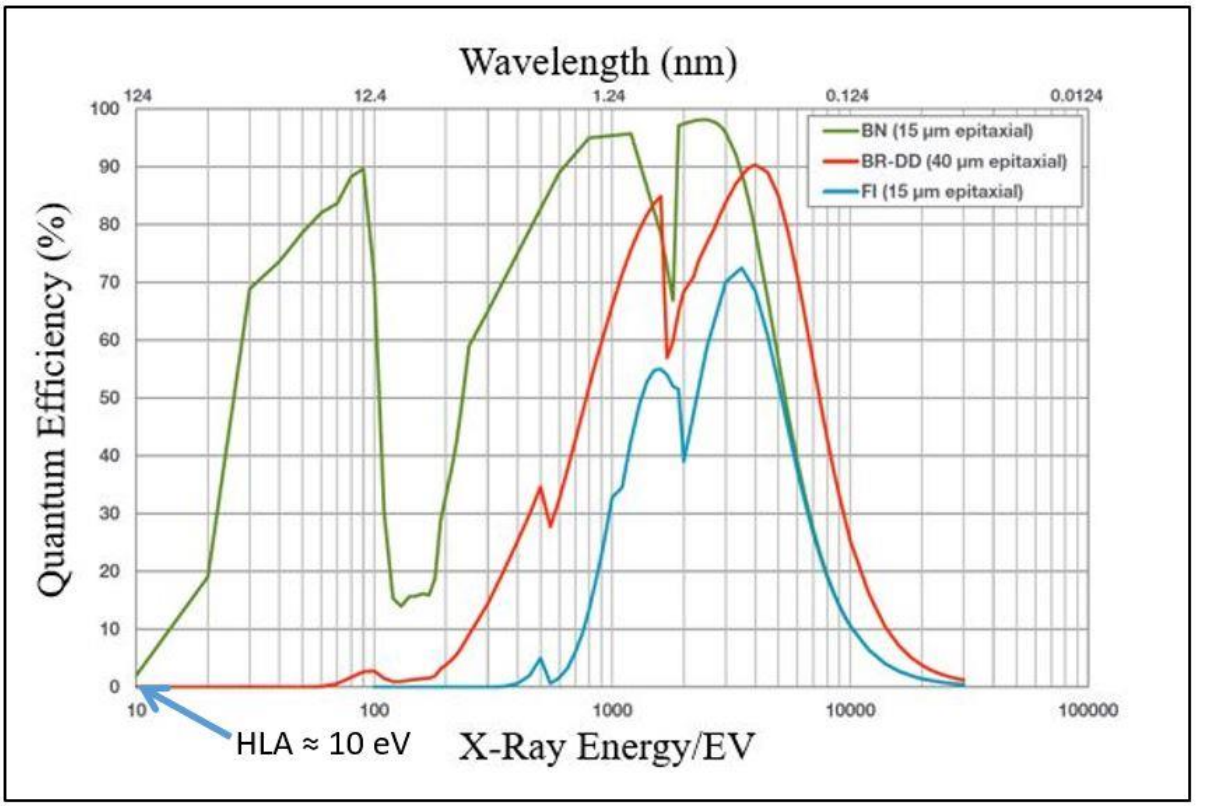

Fig. 6 Quantum Efficiency of Andor iKon-M SO. The model used in this application is a back-illuminated sensor with no AR coating (BN), which follows the green curve

The Thermo-electric (TE) cooling system is used to cool the sensor from -10° C to -100° C, minimizing dark current and creating a low noise readout. High frame rates can also be achieved with a maximum pixel readout of 5MHz. Data is transferred with a USB cable and the camera can be controlled using the Andor Solis software.

5. Objective Lens Design Specification

The availability of high-quality optical material in the VUV spectral range is extremely limited [5]. Optical materials that are transparent in this wavelength range are MgF_2 and LiF [7]. However, the birefringence of MgF_2 is 4.44×10^{-3} at the 121.6nm wavelength, which excludes MgF_2 as powerful optical elements due to the excessive polarization aberration [8]. LiF is optically isotropic, but the high transmission of LiF in the VUV spectral range depends on the material purity, growth process, polishing, storing and handling of the crystals and is hard to obtain [9]. Thus, reflective mirrors are used as focusing elements in this system to limit chromatic aberration. The specification of the system is summarized in Table 3. A Schwarzschild design with two spherical mirrors is selected to work with a moderate numerical aperture of 0.3 [11][13]. The diffraction limited Airy disk size of this system is about 250nm. The camera pixel size specification requires the diffraction-limited system magnification to be 120x for a sufficient sampling in the imaging plane. Limited by the sensor size, the FOV in object side is ±80μm. The focal length of the objective is set at 10mm to prevent an excessive system length with the 120x magnification, while avoiding manufacturing very small mirrors to maintain 0.3 NA

.

Table 3. System specification

Configuration	Schwarzschild
Source Spectrum	121.6nm (FWHM 3pm)
Objective Conjugate	Finite
Magnification	120x
NA	0.3
Focal Length	10mm
Radius of Curvature of Primary Mirror	36.873mm
Radius of Curvature of Secondary Mirror	12.686mm
Mirror Spacing	23.788mm
Clear Aperture of Primary Mirror	28.6mm
Clear Aperture of Secondary Mirror	6mm
Central Obscuration	2.4mm
Working Distance	5mm (Dry Air)
Total Length between Object and Image Plane	1234mm
FOV (object)	±80 μm
Sensor Size	13.3×13.3 mm
Pixel Size	13×13 μm
Temperature	20°C
Pressure	<100 mtorr (inside chamber)

6. Illumination Scheme

The microscope is divided into two main sections, which are the illumination path and the imaging path. The illumination path consists of the HLA source, illumination optics, the objective lens, and the sample plane. The spatial and angular distribution of the VUV source is assumed uniform, and the illumination method is critical illumination. Using only one lens, the critical illumination scheme throws away at least 40% of light due to the obscuration. Critical illumination is designed so that the source is reimaged to the object plane with proper magnification. A stock f = 90.13mm, MgF_2 lens (LA6006, Thorlabs Inc.) is selected according to the mechanical dimensions. Critical illumination, where the extended source is directly imaged onto the sample plane, is shown in Fig. 7. Each point on the source is treated as a point source, which produces an irradiated spot on the sample that has a size according to the illumination system's point spread function. The total sample illumination irradiance is the integral of all of the incoherent point spread functions over the sample plane.

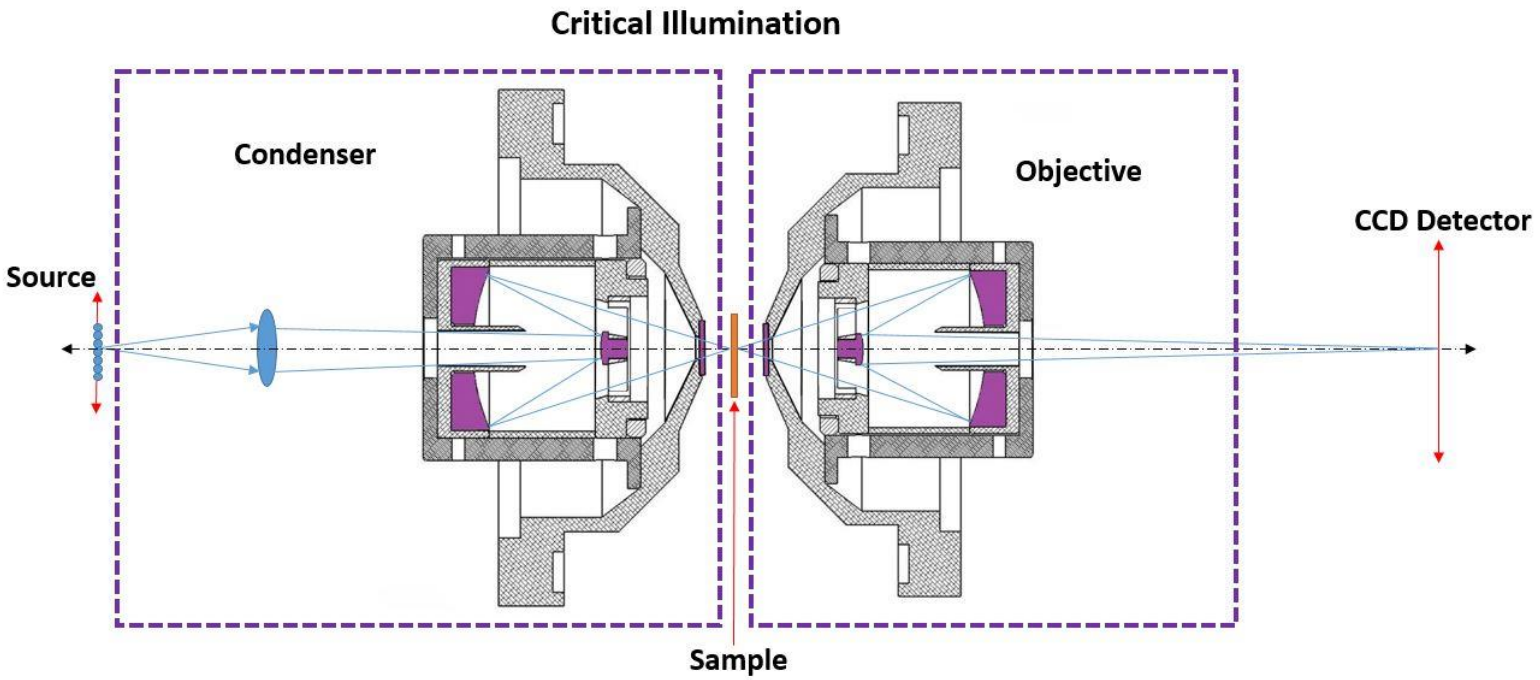

Fig. 7 Critical Illumination Scheme

The HLA source is used with an Acton Optics MVUVBS45-1D spectrally narrow bandpass filter that attenuates the non-121.6 nm light according to the plot shown in Fig. 8. Since the source emits from a gas medium of neon and hydrogen, there are spectral neon lines that will pass through the filter. The optomechanical illumination design is shown in Fig. 9. The condenser system consists of a MgF2 lens with a focal length of 90.13 mm at $\lambda = 121.6$ nm, and the objective lens. The distance between the emission point to the lens and the centration of the emission point to the optical axis is critical in creating the optimal illumination field on the sample plane. Therefore, a small compliant bellow attaches the lamp to the microscope housing. Fig. 9 illustrates the modeled illumination configuration of the microscope. The MgF2 lens is mounted inside of a 4-inch threaded lens tube, which can be adjusted inside of the 4 way cross. The beam splitter is mounted into a tip-tilt adjustable mount.

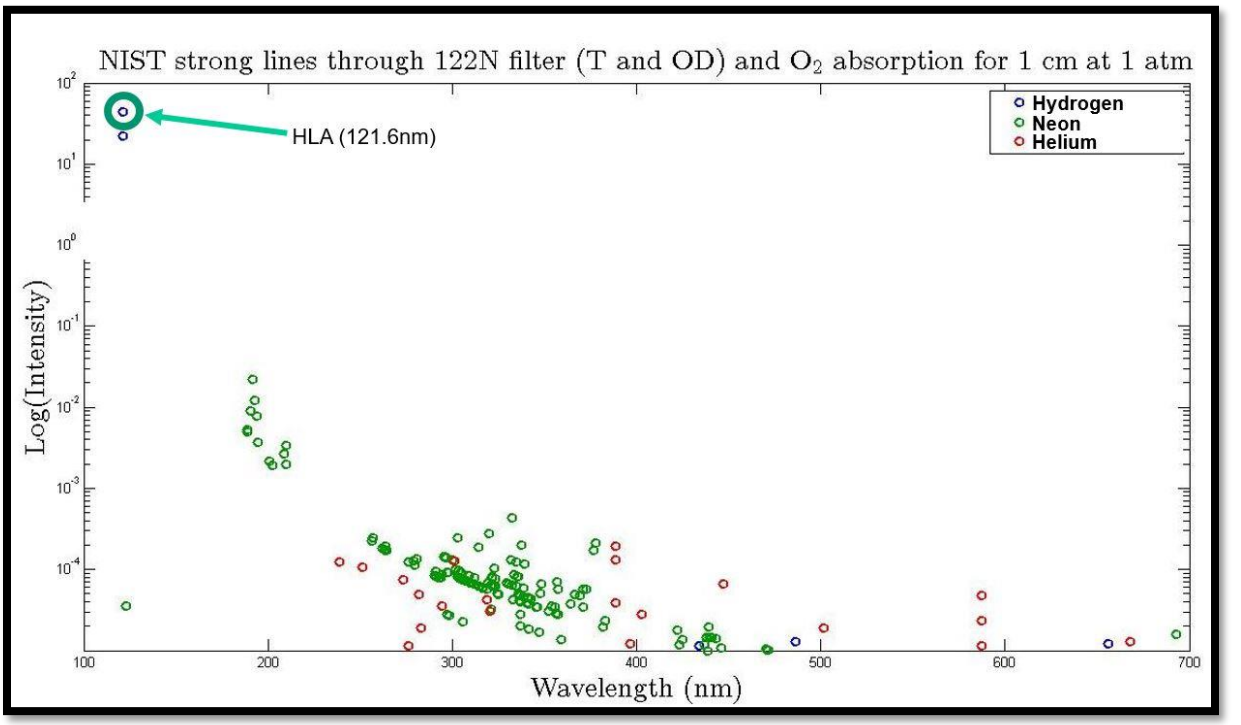

Fig. 8 Hydrogen, Neon, and Helium Spectral lines through filter

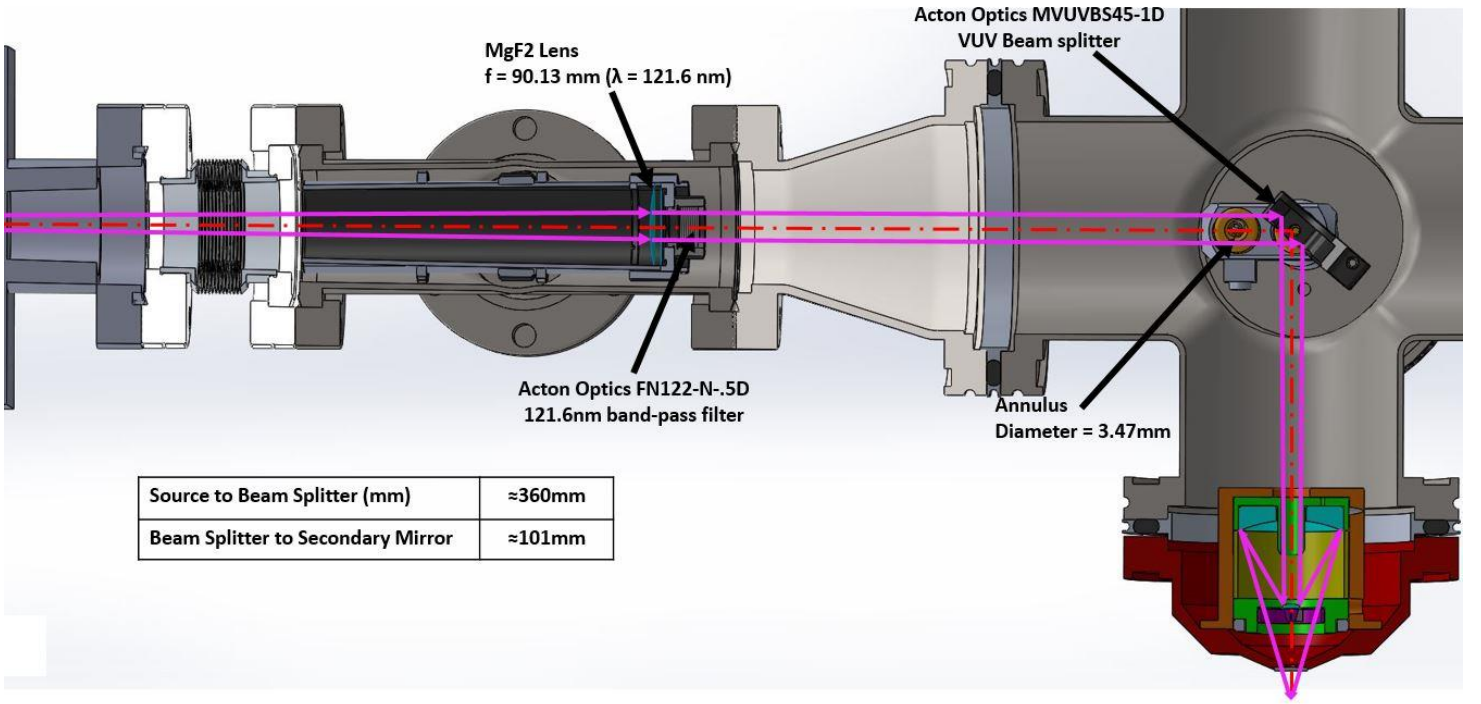

Fig. 9 Model of the illumination method

7. Optical Design

To maintain high transmission and prevent contamination, a vacuum window is placed close to the sample plane that leaves the majority of optical path inside a vacuum chamber. MgF_2 introduces intolerable polarization aberration in the path of a converging beam with undefined source polarization. Even though more hygroscopic and mechanically softer than MgF_2, LiF becomes the only window selection for this wavelength [12]. To reduce the contamination and degradation of the material, the front side of the 1mm LiF plane parallel flat is covered with a customized nitrogen-purged storage seal box when the system is not in operation. Inside the chamber, a low vacuum is maintained to secure high transmission of the VUV wavelength while providing a clean environment for the optical system.

The layout of the optical system is shown in Fig. 10. A concave primary mirror and a convex secondary mirror are placed so that minimal coma and astigmatism are generated while spherical aberration is over-corrected to compensate the residual spherical aberration from the LiF window [13]. The illumination path from the source is reflected from a 2.5mm thick MgF_2 beam splitter where the imaging path passes through the beam splitter towards the CCD detector. Since the imaging path passes through the birefringent material of the beam splitter, polarization aberration is introduced into the image. However, the induced aberration from a 2.5mm c-cut MgF_2 plate only has a 0.06 reduction in Strehl Ratio, which has little effect on maintaining diffraction limited performance of the system.

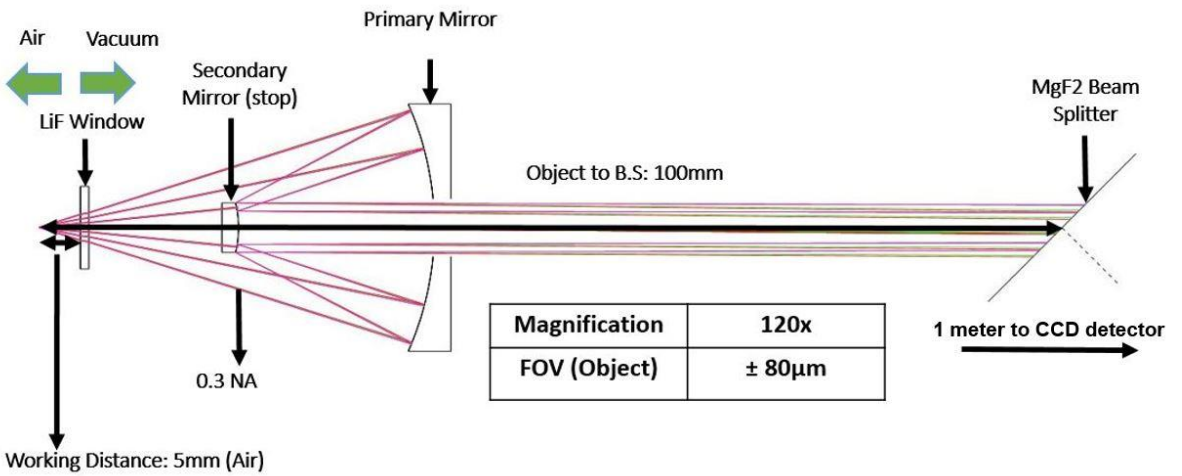

Fig. 10 Optical layout of the system. The incoming illumination path and imaging path from beam splitter to the image plane is ignored.

Optical performance is shown in Fig. 11 with RMS wavefront error vs field height. Even though the rotational symmetry is broken by the tilted beam splitter, the rotationally symmetric optical performance plots are representative by realizing the fact that the asymmetric wavefront perturbations introduced by the beam splitter are insignificant over all field angles. It is worth mentioning that the plot of Fig. 11 is analyzed with a reversed system, where data in the object plane are plotted. The residual Petzval curvature is balanced by moving the CCD detector plane away from Gaussian image plane. The minim wavefront error is achieved at 0.7 field, due to the nature of the quadratic dependency of the Petzval curvature with respect to the field height.

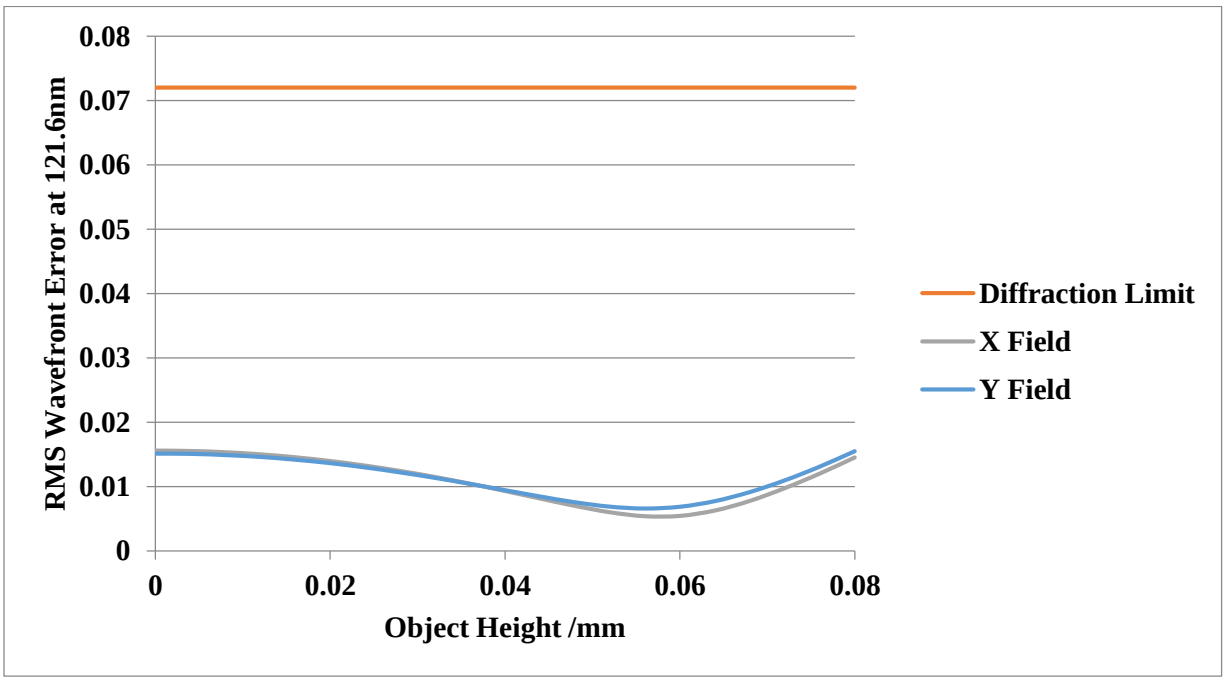

Fig. 11 RMS wavefront vs field height

8. Tolerance Analysis

Before defining the fabrication specifications of the optical and mechanical components, a tolerance analysis is performed in CodeV optical design software. Compensators include defocus, axial spacing between mirrors and the lateral displacement of the secondary mirror. The mirror spacing is adjusted and set with a precision metal shim. Lateral displacement of the secondary mirror is achieved by precision adjustment screws. A sensitivity analysis using on-axis Strehl Ratio as the figure of merit shows that transverse decenter of the secondary is the most sensitive parameter, which is followed by axial separation between the primary and secondary mirror. Figure 12 shows reduction in Strehl Ratio with respect to decenter of the secondary mirror. To maintain an on-axis 0.8 SR (diffraction limited), the secondary mirror has a +/- 6 μm decenter tolerance with respect to the primary mirror positon. To have a performance safety factor, the secondary is aligned to +/- 3 μm decenter to maintain a > 0.9 on-axis SR.

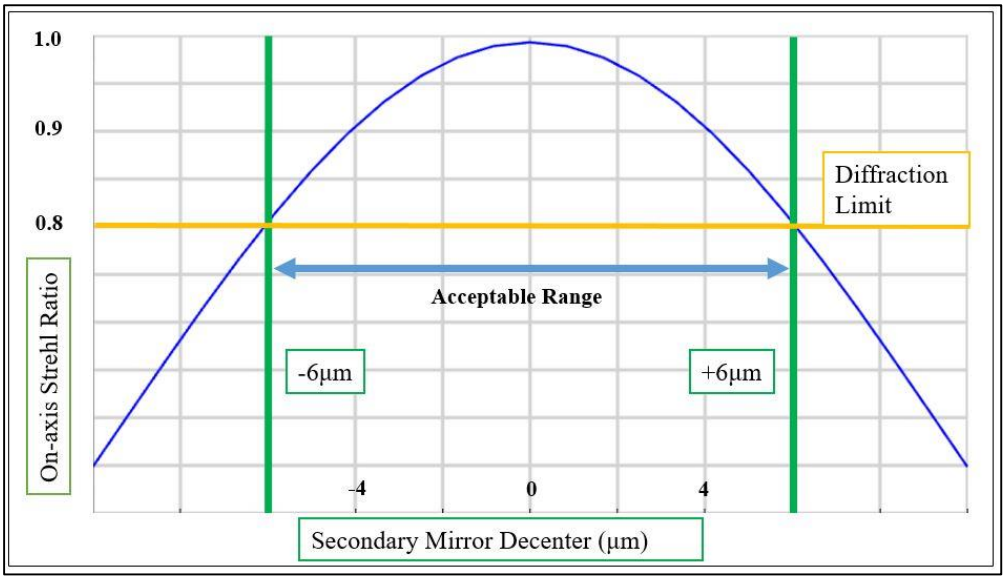

Fig. 12 On-Axis Strehl-Ratio vs. Secondary Mirror Decenter

The primary and secondary mirror radius errors from nominal value are compensated with defocus and spacing between the two mirrors. The primary and secondary mirrors are both spherical. Therefore, the mirror wedge (usually interpreted as total indicator runout) and decentering can be compensated with lateral displacement of the secondary mirror. The optical performance for a perfectly aligned system compared to a system with maximum allowed tolerance deviations is shown in Fig. 13 in the form of spot diagrams. Black circles represent Airy disk diameters, which in this case are 240 nm in diameter at the object with 121.6 nm light. Figure 13 illustrates diffraction limited performance with a + 6 µm transverse decenter of the secondary, and a – 10 µm axial spacing error between the primary and secondary mirror vertices.

Image performance is very sensitive to the residual surface errors from the fabrication process in short wavelength systems. A Wavefront Differential Tolerance Analysis (WDTA) with 30nm surface figure error in both surfaces is shown in Fig. 14. CodeV's WDTA assumes that the overall performance follows a Gaussian Distribution [23]. The wavefront error at mean + 2σ (95% probability) is barely within the diffraction limit. This sets the RMS surface figure error tolerance at the range of 5nm (30nm +/- 2.5nm).

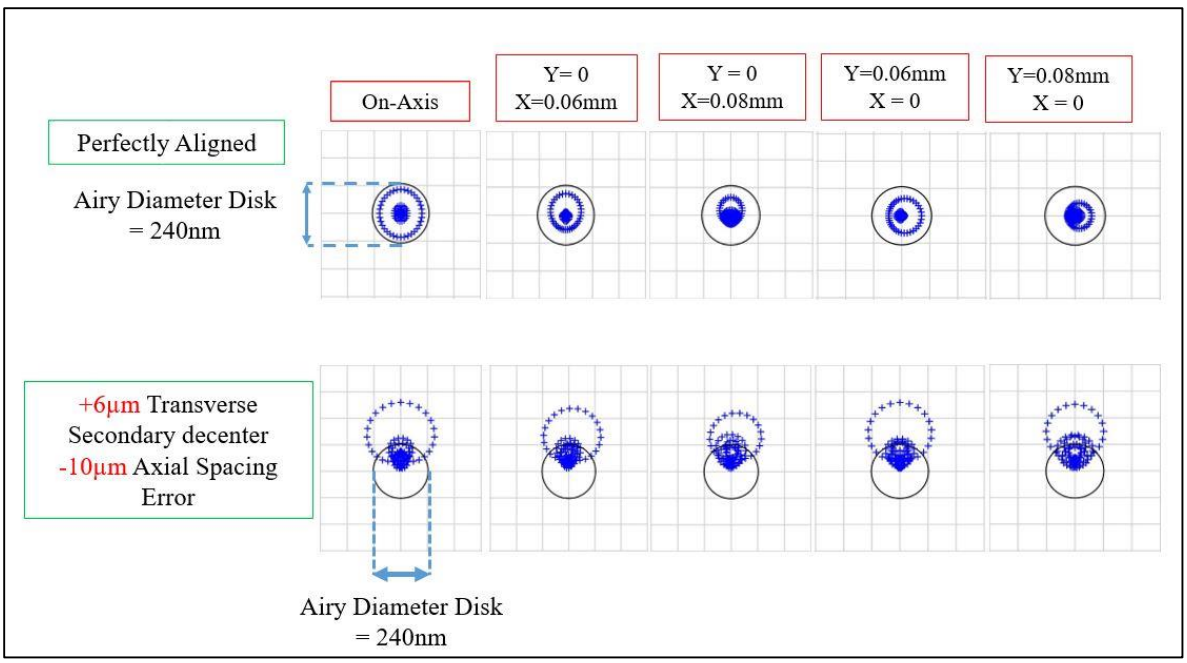

Fig. 13 Spot diagram for a perfectly aligned system. (Top) Spot Diagram for maximum tolerance mirror deviations (Bottom).

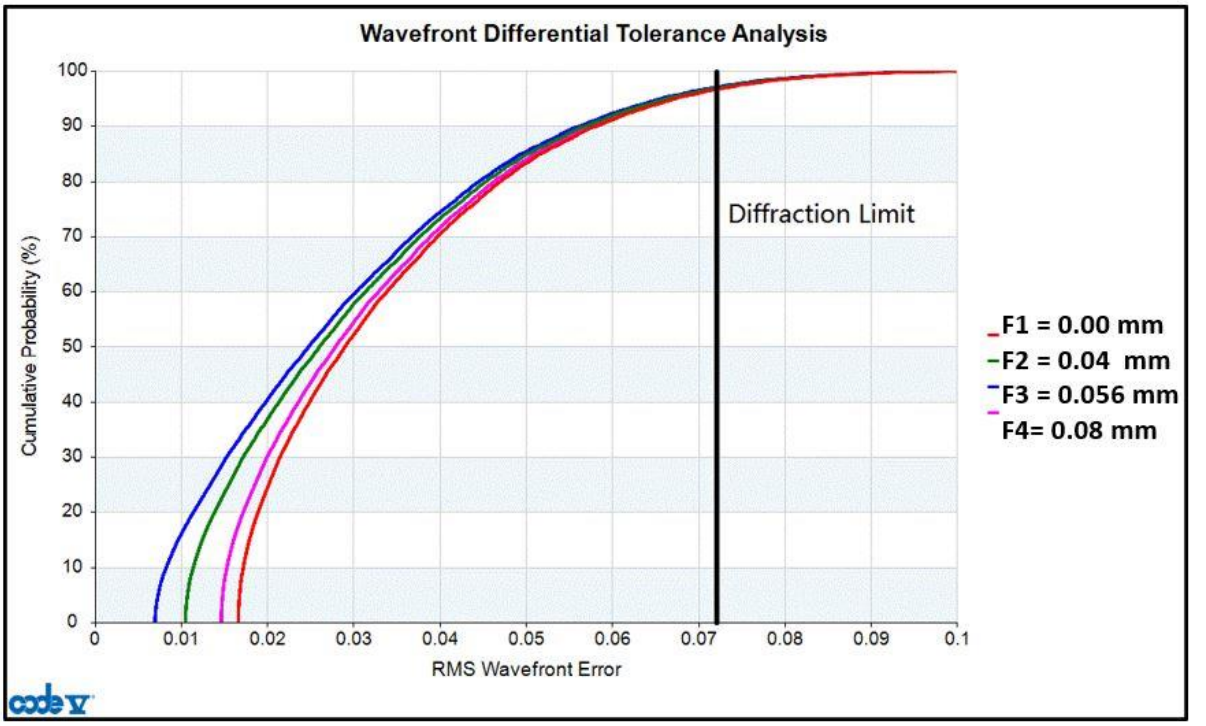

Fig. 14 Wavefront Differential Tolerance analysis with 30nm surface figure error on primary and secondary mirror for Field heights 0 mm, 0.04mm, 0.056 mm and 0.08mm (full field)

9. Mirror Fabrication

The Primary and Secondary mirror are fabricated using a Nanotech 450 UPL single-point diamond turning (SPDT) machine at the Korea Basic Science Institute [22]. The mirrors are fabricated from high purity RSA 6061 Aluminum with surface roughness of 2nm, which is at the state-of-the-art performance for SPDT machines [10]. Surface roughness measurements of the primary and secondary mirrors taken by a Wyko optical profilometer NT 2000 are shown in Figs. 15 top and 16 top, respectively. RMS surface roughnesses of the primary and secondary mirrors are 1.43nm and 1.83nm, respectively. High spatial frequency errors (micro-roughness) are excluded from the image performance analysis of Fig. 14. To limit the effects of scattering, based on Eq.(1), a surface roughness of $\lambda/1000$ is necessary to limit the optical scattering to around 0.1% of the incident light. Due to limitations in SPDT technology, the minimum achievable surface roughness is roughly 2nm, which is $\lambda/100$. A classical definition of total integrated scatter (TIS) is used to quantify the power loss due to scatter from the mirror's surface roughness. TIS describes a functional relationship between surface roughness and optical scattering [24].

$$TIS = 1 - e^{-\left(\frac{4\pi \cos(\theta_i) R_q}{\lambda}\right)^2} \qquad (1)$$

In Eq.(1) θ_i is the angle of incidence to the surface normal, R_q is the surface RMS roughness, and λ is the wavelength. This calculation is based on the marginal ray, which exhibits an angle of incidence for the primary mirror and secondary mirror of 0.089 radians and 0.297 radians, respectively. The marginal ray has the largest angle of incidence on the mirror surfaces, so this calculation presents the worst case TIS

scenario. These values are calculated using equations (2) and (3), which are determined using Figs. 15 bottom and 16 bottom, respectively.

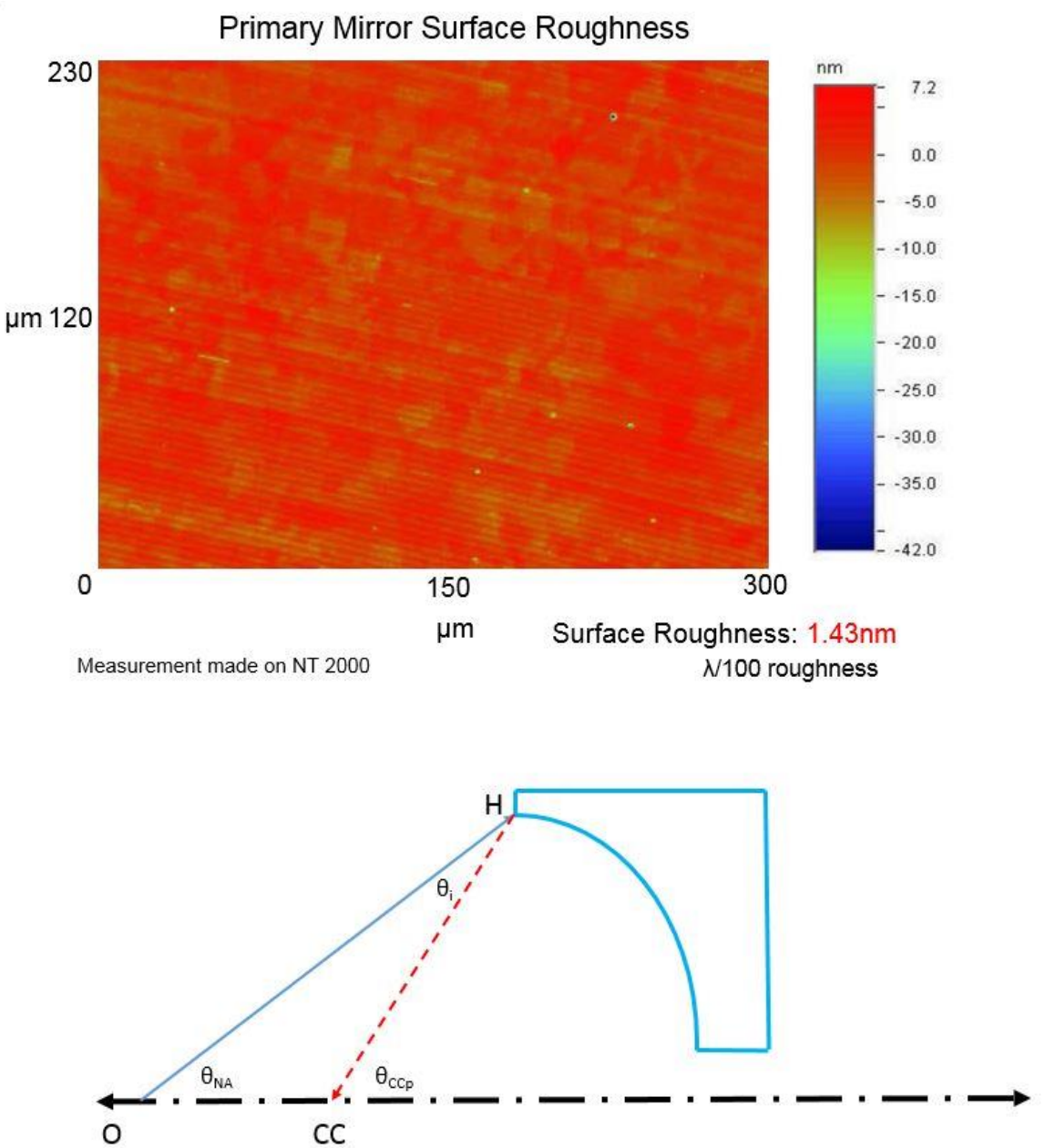

Fig. 15 (Top) Primary mirror surface roughness (Bottom) Schematic for primary TIS calculation

$$\frac{\overline{OCC}}{sin(\theta_i)} = \frac{\overline{HCC}}{\sin(\theta_{CCp})} \qquad (2)$$

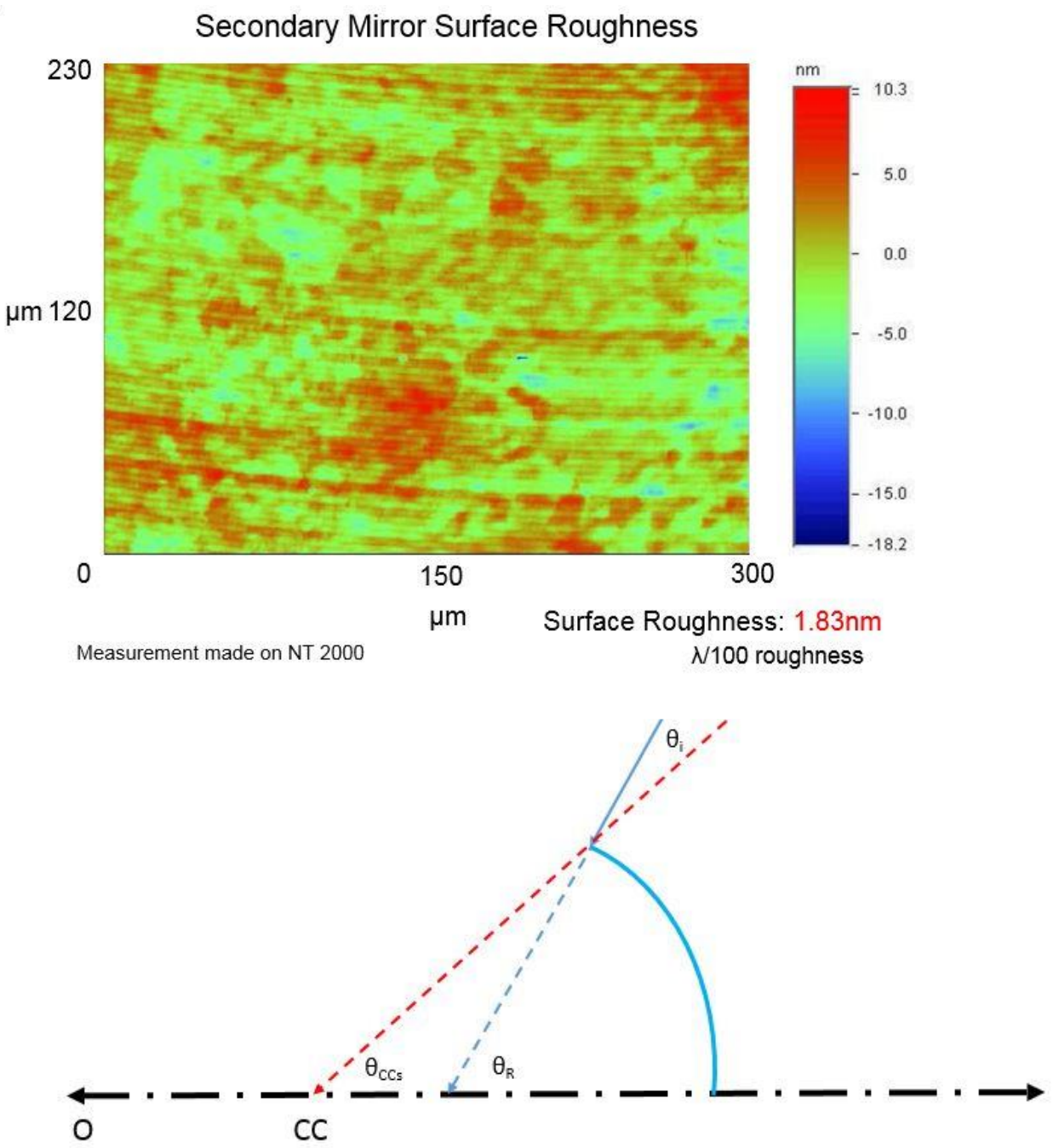

Fig. 16 (Top) Secondary mirror surface roughness (Bottom) Schematic for secondary TIS calculation.

$$\theta_i = \theta_R - \theta_{CCs} \qquad (3)$$

The TIS of the primary mirror is 0.021(2.1%), and the TIS of the secondary mirror is 0.033 (3.3%). The stray light control in the system is discussed later in the thesis, but the main effect that the TIS will have on imaging is loss of illumination throughput.

Interferometric tests of the primary and secondary mirror surfaces are shown in Fig. 17. The RMS figure errors are 12.0 nm for primary mirror and 8.9 nm for the secondary mirror, which exceeds the tolerance value to maintain diffraction limited performance. However, by adjusting the relative orientation of the mirrors, which is called "clocking", the asymmetric figure errors partially compensate each other and results in much better overall spatial frequency resolving capability compared to randomly assembled mirror sets.

a) 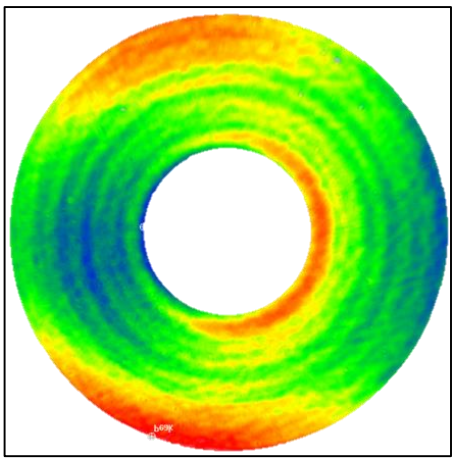

b) 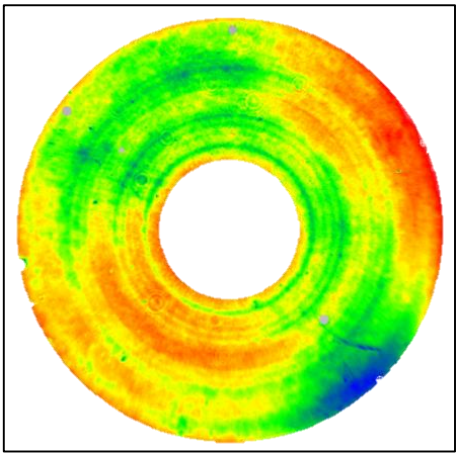

Fig. 17 (a) Surface interferogram primary mirror (b) secondary mirror.

To clock mirrors, the figure error of each surface is first measured. Fiducial marks are placed on both mirrors so that they define orientation of the surfaces. Then, surface figure errors are fit with fringe Zernike polynomials and are exported to the optical design software. Orientation of one surface (gamma angle) is optimized for best optical performance. An example is shown in Fig. 18. The compensation of “high” and “low” surface figure is clearly seen from the properly oriented mirror set. Improvement of the system performance is shown in MTF plots. The optimized angle of orientation is recorded for use with the alignment process.

a) 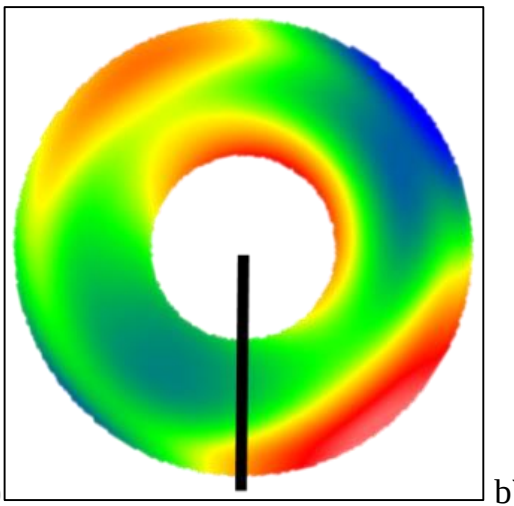

b) 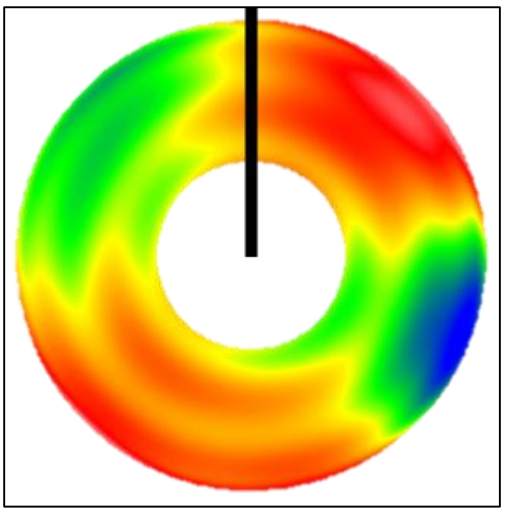

c) 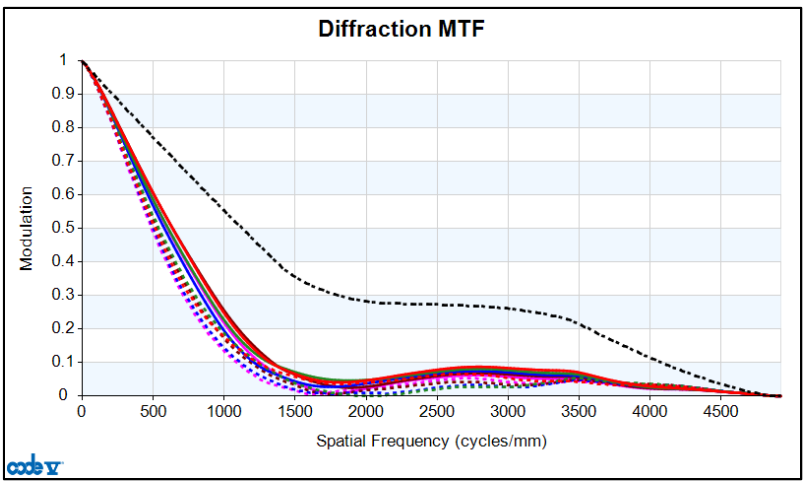
Diffraction MTF
Modulation
1
0.9
0.8
0.7
0.6
0.5
0.4
0.3
0.2
0.1
0
0
500
1000
1500
2000
2500
3000
3500
4000
4500
Spatial Frequency (cycles/mm)
code V

d) 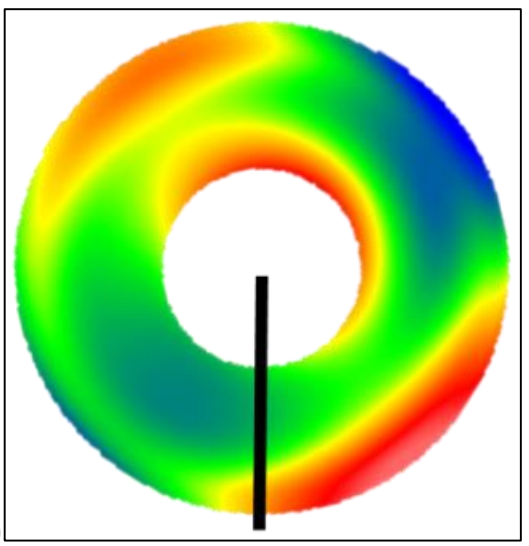

e) 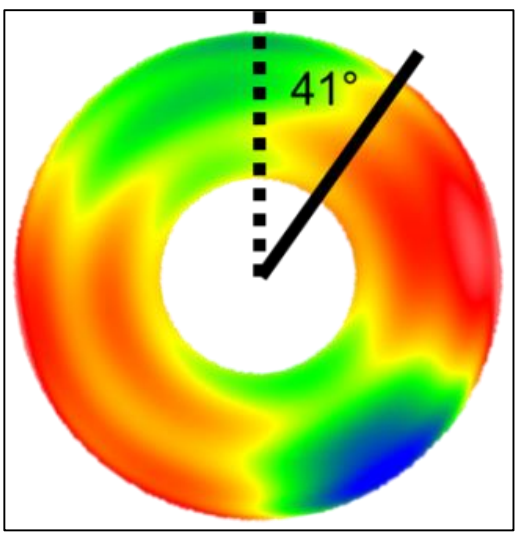
41°

f) 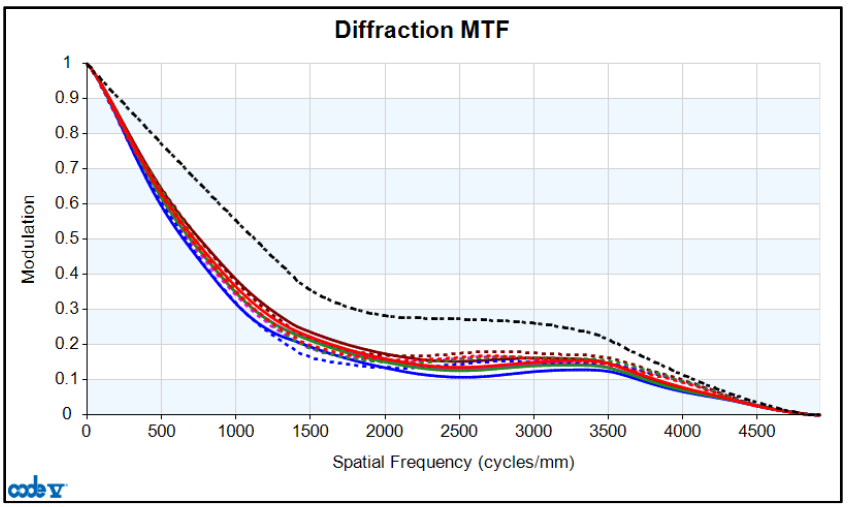

Fig. 18. a) Primary and b) secondary mirror surface figure without clocking, c) MTF chart without clocking; d) primary and e) secondary mirror with clocking, f) MTF chart with clocking.

10. Optomechanics

The purpose of the mechanical components in an optomechanical system is to control positions of the optical elements with their respective tolerances based on tolerance analysis of the optical design. The approach that is taken in order to design a cost effective high performance mechanical system is a modular technique. As explained in the previous section, the most sensitive parameters to control are the axial spacing between primary and secondary mirror vertices, the transverse decenter of the secondary mirror relative to the primary mirror, the surface figure error of the mirrors, and the surface roughness of the mirrors. The last two parameters are a byproduct of the quality of the diamond turned mirrors, and are not necessarily controlled by the mechanical housing. Therefore, the mechanical packaging must control the other two parameters within their respective tolerance ranges in order to achieve optimal performance.

The HLA mechanics are designed using Solidworks 3-D CAD modeling software. The optical system is imported into the CAD software, and it is treated as a reference for the design of the mechanical elements. An important step that is followed when designing the optomechanical system is the consideration of the alignment procedure that will be followed when assembling the system. Another important consideration is the manufacturability of the designed components.

The optomechanical system is composed of 9 elements: the objective barrel, primary mirror, secondary mirror, primary mirror cell, secondary mirror cell, secondary spider, spacer, retainer ring and the vacuum cap. The CAD model is used as an accurate tool for determining mechanical dimensions for controlling the set optical parameters. The assembled model is shown in Figs. 19 and 20. Each of the mirrors are mounted into their own cells. The cells are then stacked inside the barrel and are separated by a spacer. The axial spacing tolerance is controlled and fixed by the spacer and the shim. The transverse decenter of the mirrors are controlled using 8 radial adjustment screws along the outside of the barrel. The primary mirror cell is adjusted using MSC P/# 64101785 M3x0.5 screws that have been customized to have a spherical tip, and the secondary mirror cell is adjusted using Base Lab Tools, TS3-010-008, M3x0.1 spherical tipped screws. The inner diameter of the primary mirror is fabricated larger than the maximum allowable tolerance. Due to the error, the alignment procedure, which is discussed in section 12, is altered to partially compensate for the unexpected error. In order to achieve sub-micrometer control for the decenter of the secondary, the adjustment screws have 254 threads per inch, which is 100 µm/revolution or roughly 0.3 µm sensitivity. During the alignment of the objective lens, the barrel is pointing in zenith, and in operation the barrel is horizontal; in order to maintain the axial position of the cells, a retainer ring is threaded onto the entrance of the barrel.

The LiF window is designed to not fracture, or exhibit any optically significant deflection due to the ≈ 759 torr pressure differential across the clear aperture. With a safety factor of 4, the minimum required thickness of the LiF window to not fracture is 0.35 mm which was determined by Eq.(4). The thickness of the LiF window is 1 mm, which is 3 times the minimum thickness. A 759 torr pressure differential across a 1mm thick LiF window will produce a maximum displacement of roughly 0.2fm or λ/1000 optical path difference (OPD), which was determined using Eq.(5) [14].

$$T = 0.5 * D * \left(K_w * SF * \frac{\Delta P}{\sigma_s} \right)^{\frac{1}{2}} \qquad (4)$$

$$\delta = 0.00889 * (n-1) * \frac{\Delta P^2 * D^2}{E_g^2 * T^2} . \qquad (5)$$

T = minimum required thickness ΔP = Pressure differential SF = Safety Facto
σ_s = Apparent elastic limit δ = maximum OPD change K_w = Unclamped constant
D = Optical element clear aperture E_g = Young's Modulus
n = Refractive index

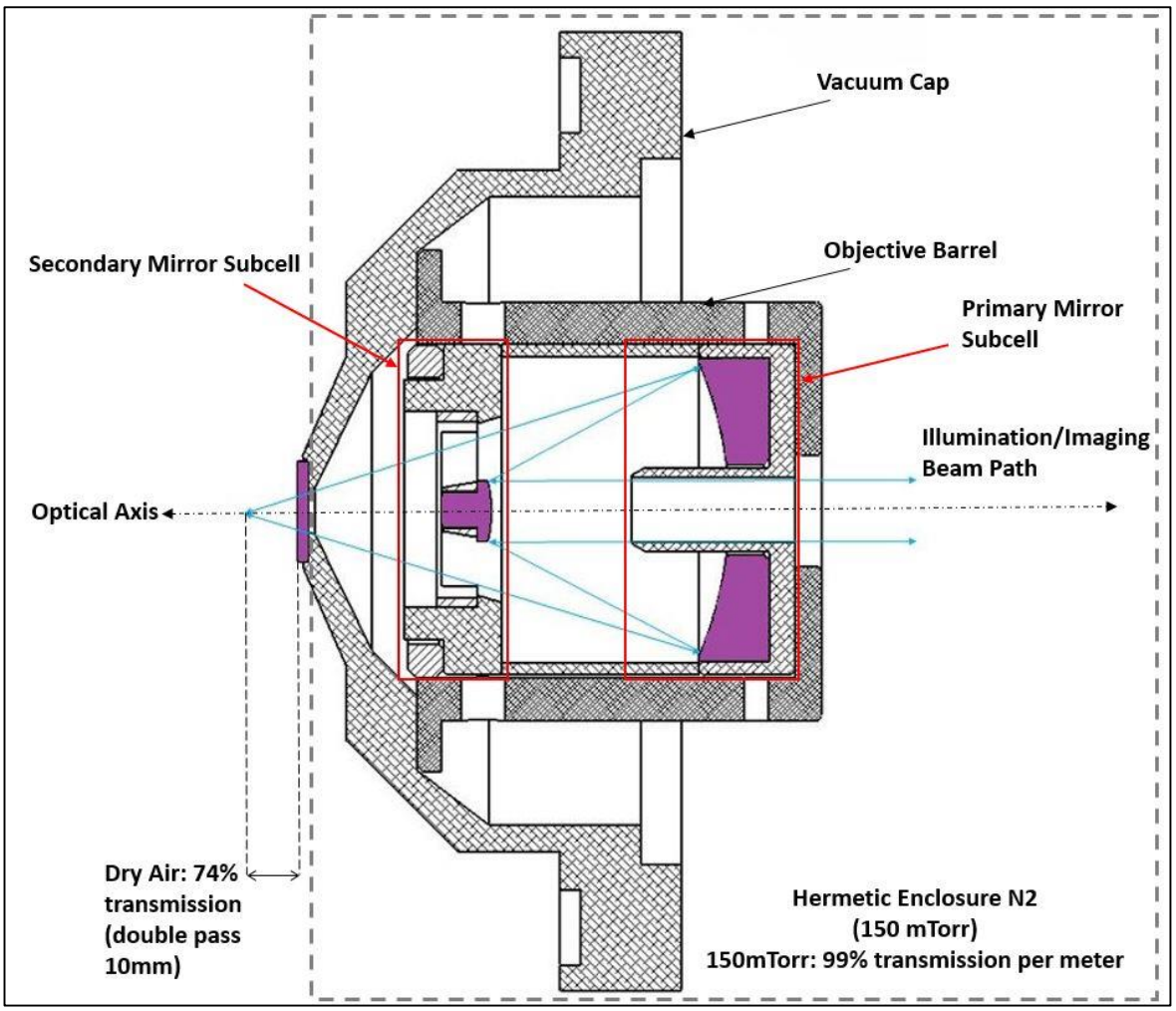

Fig. 19 HLA Objective (Purple defines optical components)

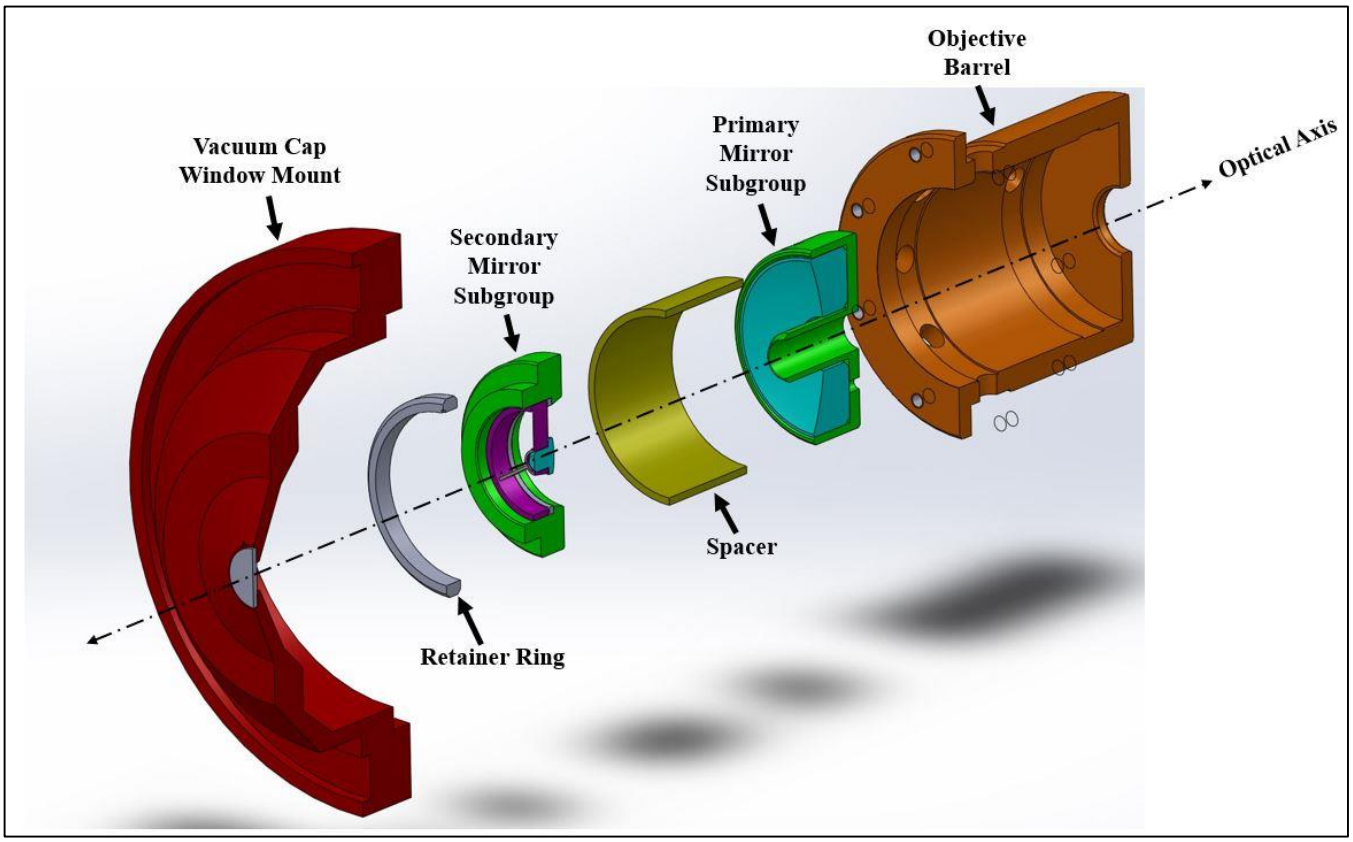

Fig. 20 Exploded model of the HLA Objective Lens

The optical and mechanical components, except the LiF window, are machined from aluminum alloys that have matching coefficients of thermal expansion (CTE). The microscope operates in a thermally controlled environment, and the optical and mechanical components have similar CTE's. Therefore, an in-depth thermal analysis is not completed. To calculate the displacement of the objective lens due to gravity, a first-order FEA is simulated. The model consists of the objective barrel constrained to the fixed geometry of vacuum cap. Weights of the individual components are in Table 4. Force is equal to the mass times the acceleration. If gravity is the only acceleration considered, which is a good approximation for the system, the total force is 9.706 N.

This force creates a deformation of the barrel with respect to the vacuum cap. The max displacement of the barrel due to gravity is 19.47 nm, which is shown in Fig. 21. This displacement is insignificant with respect to the alignment tolerances.

Table 4. Weight of Objective components

Mechanical Element	Weight (grams)
Primary Mirror	9.84
Secondary Mirror	0.18
Primary Cell	8.6
Secondary Spider	11.04
Secondary Cell	2.15
Spacer	6.44
Barrel	60.79
Total	99.04

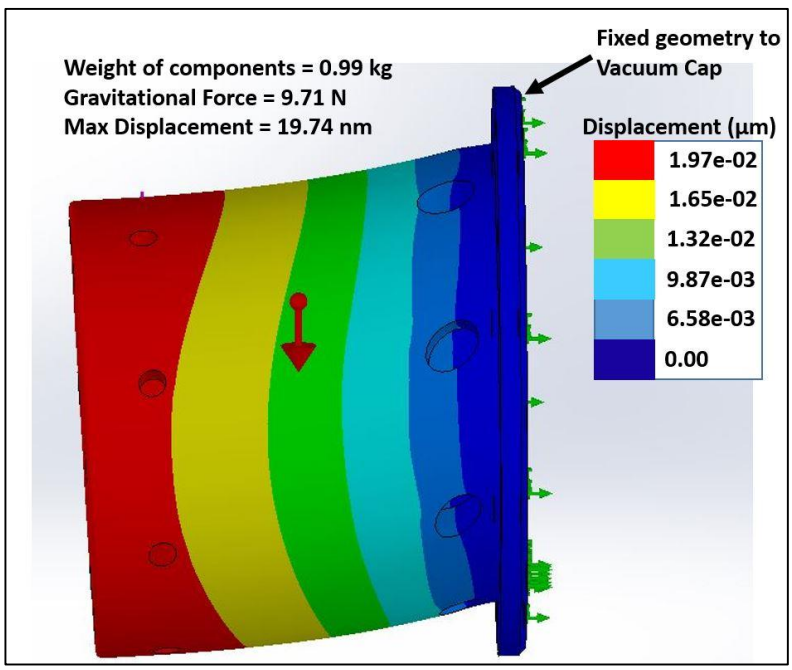

Fig. 21 Objective Barrel Displacement due to gravitational load. The max displacement based on the FEA is 19.74 nm, which will not affect image motion beyond specification.

10.1 Primary Mirror Cell

The main purpose of the primary cell is to securely mount the primary mirror. There is ± 50 µm clearance between the outer diameter of the primary mirror to the inner diameter of the primary mirror cell. The design drawing for the component is shown in the Appendix C. The important tolerances are with respect to the datum surface C, which allows for reference surface stacking from the barrel to aide in the alignment.

The primary mirror cell is also designed to control unwanted stray light from various scattering sources with an optimized baffle design. The design on the baffle is explained in the stray light section 11.

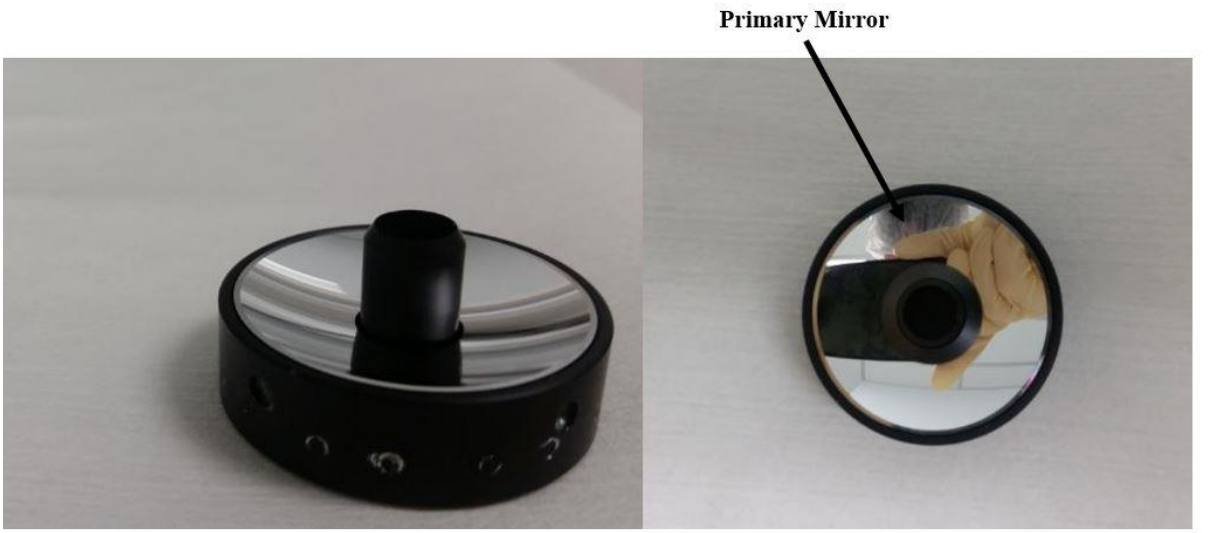

Fig. 22 Fabricated Primary Cell

10.2 Secondary Spider Mount

The secondary mirror is potted with Double Bubble two-part Urethane into a 3 arm spider mount. The width of the spider mount's arms are 0.5 mm. The loss of light due to the arms is 4.1%. The simulated geometric effects from the spider arms on the CCD image plane from a uniform point source illumination is shown in Fig. 23. The simulation uses non-sequential Zemax. 10 million rays were traced from the sample plane to the CCD detector through the optical system with only the addition of the spider arms as an obstruction. The secondary spider is designed to mount directly into the secondary cell.

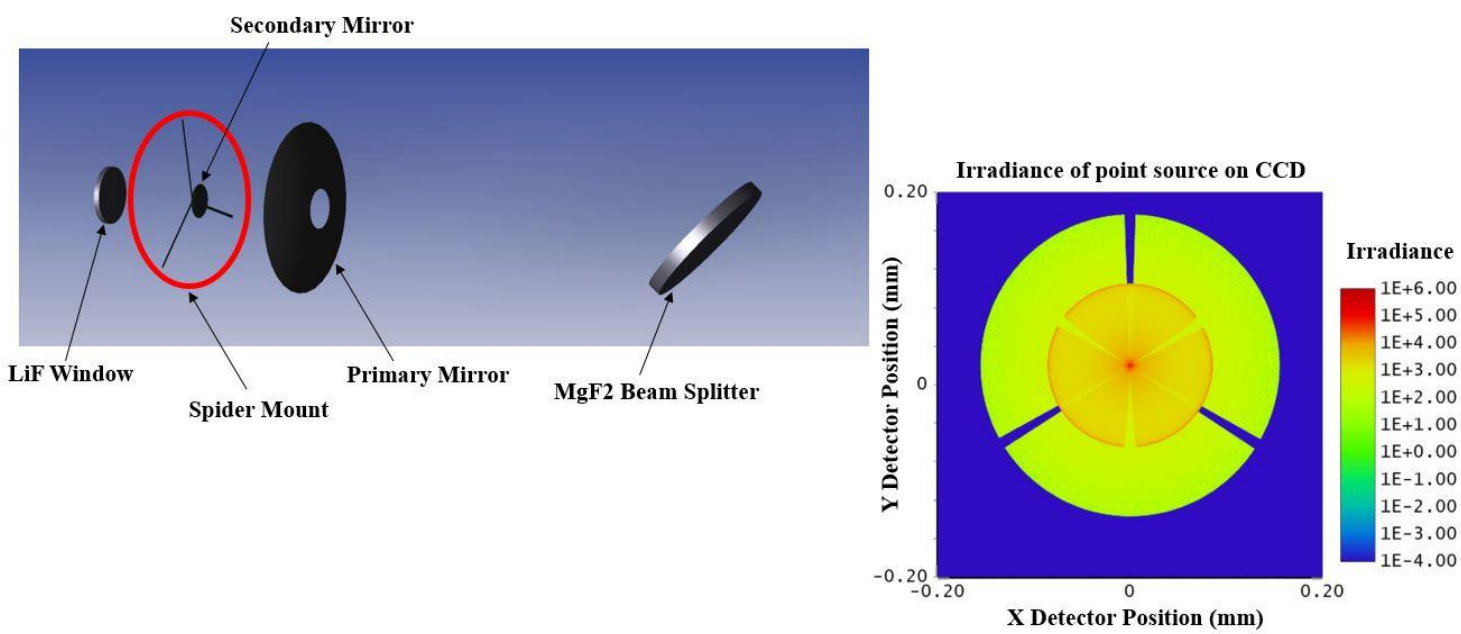

Fig. 23 Geometric effects on sample plane (Plot Log base 10 to emphasize geometric effects)

10.3 Secondary Mirror Cell

The secondary mirror cell is designed to mount the secondary spider. The entrance aperture of the cell has a beveled surface that is similar angle to the NA of the objective lens. The back half of the cell is designed to allow the retainer ring to press against the cell in order to apply a compressive force after the alignment and assembly is complete. The assembled secondary subgroup is shown in Fig. 24.

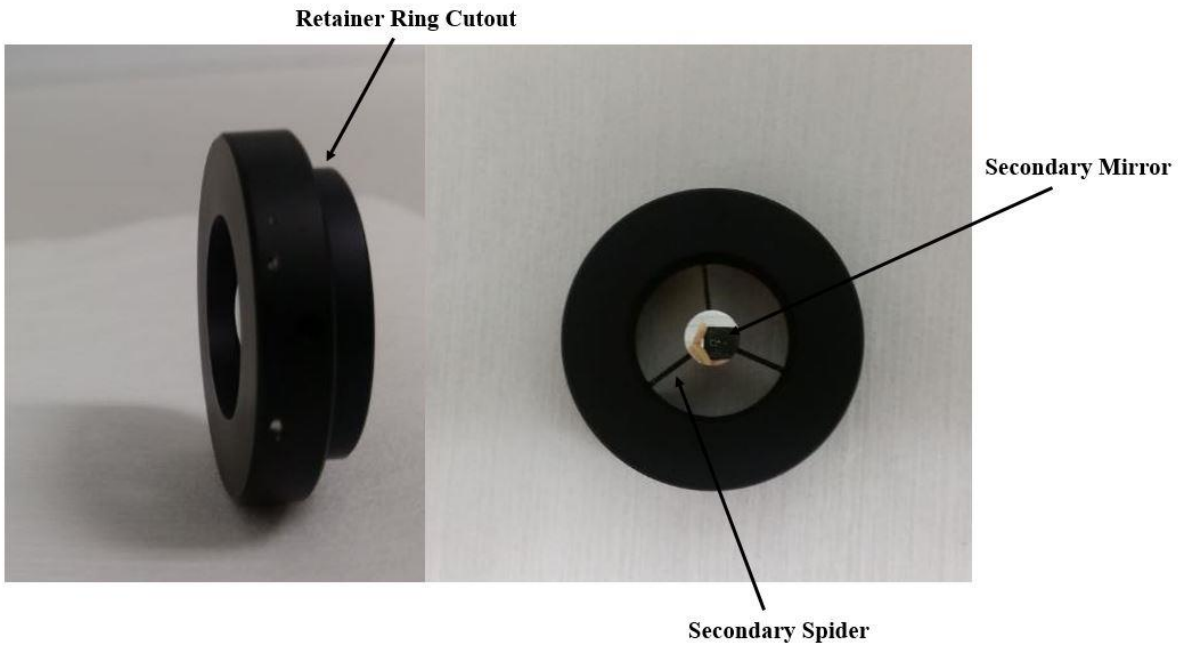

Fig. 24 Assembled Secondary Subgroup

10.4 Objective Barrel

The objective barrel is designed for many purposes. The general purpose for the barrel is to create a reference construct for constraining and aligning the mirror cells. As mentioned above, the objective lens is aligned while pointing in the zenith direction. Therefore, the alignment reference surface is the bottom surface of the barrel noted as datum surface B in the drawing. There are no adjustments for tip and tilt for the mirror cells inside of the barrel, so tolerances placed on the parallelism of the inner back surface of the barrel and mirror cells are very important.

The inner diameter of the barrel is 33.4 mm +0.05 mm. The outer diameter of the mirror cells is designed to be 32.8 mm -0.05 mm. This range allows for a minimum compensation range of ± 300 µm inside of the barrel. The back surface of the barrel has 8 radial tapped holes that allow the barrel to be attached to an adapter plate that fits directly onto a five axis mount for an interferometry setup. The front surface of the barrel has 8 radial through holes that allow the barrel to attach directly to the vacuum cap from the inside.

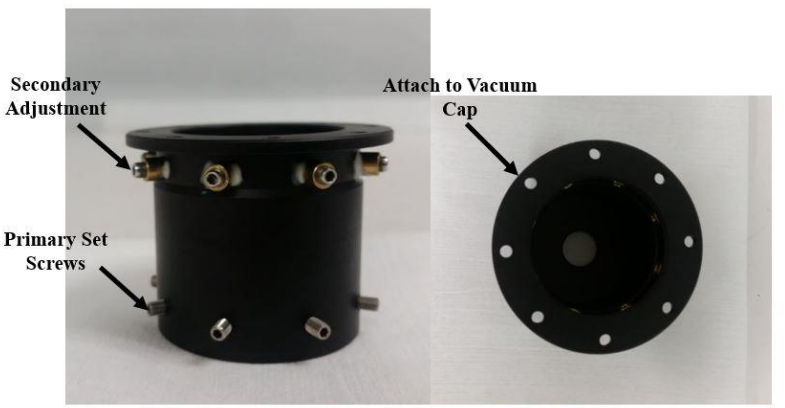

Fig. 25 Fabricated Barrel

10.5 Spacer

The spacer is designed and fabricated with a higher precision than any of the other components. This is because the spacer is designed as the compensator for the fabrication errors. The assembly of the objective lens consists of stacking the cells, then adjust the transverse decenter of the cells using radial adjustment screws. Once the cells are stacked the axial spacing between the mirrors is set. Therefore, any fabrication errors for the mechanical components will contribute to error in the axial spacing. As shown above, an important optical tolerance that the mechanics need to control is the axial distance between the secondary and primary mirror vertices to within ± 10 μm. In order to limit the amount of high precision components, the spacer is fabricated after all of the other components are fabricated and the fabrication errors are quantified.

Table 5. Optimal Spacer Thickness Design Procedure

Steps	Action	Purpose
0	Diamond Turn Primary and Secondary Mirrors	Measure important optomechanical parameters: H_Primary, H_Secondary, R_Primary, R_Secondary
1	Machine Primary and Secondary Mirror cells	Measure important mechanical parameters: H_secondary cell, H_Primary cell (see Fig. 26)
2	Optimize optical system in optical design software with measured fabricated mirror parameters	Determine optimized axial spacing between mirrors to correct for fabricated mirror errors
3	Input measured mechanical mirror cell parameters into Solidworks assembly model and determine actual spacer thickness (L)	Determine spacer thickness (L)
4	Create Spacer CAD drawing, set spacer thickness tolerance to ± .012 mm, and send drawing out for fabrication	Fabricate spacer thickness with tight tolerance in order to control the axial spacing between mirror optical tolerance requirement

This procedure limits the number of possible fabrication errors that could possibly affect the spacing between the mirror vertices to 1 element. Adjusting the distance between the LiF window and the sample plane compensates for residual alignment errors associated with the fabrication of the spacer to ± 7.5 μm of thickness error.

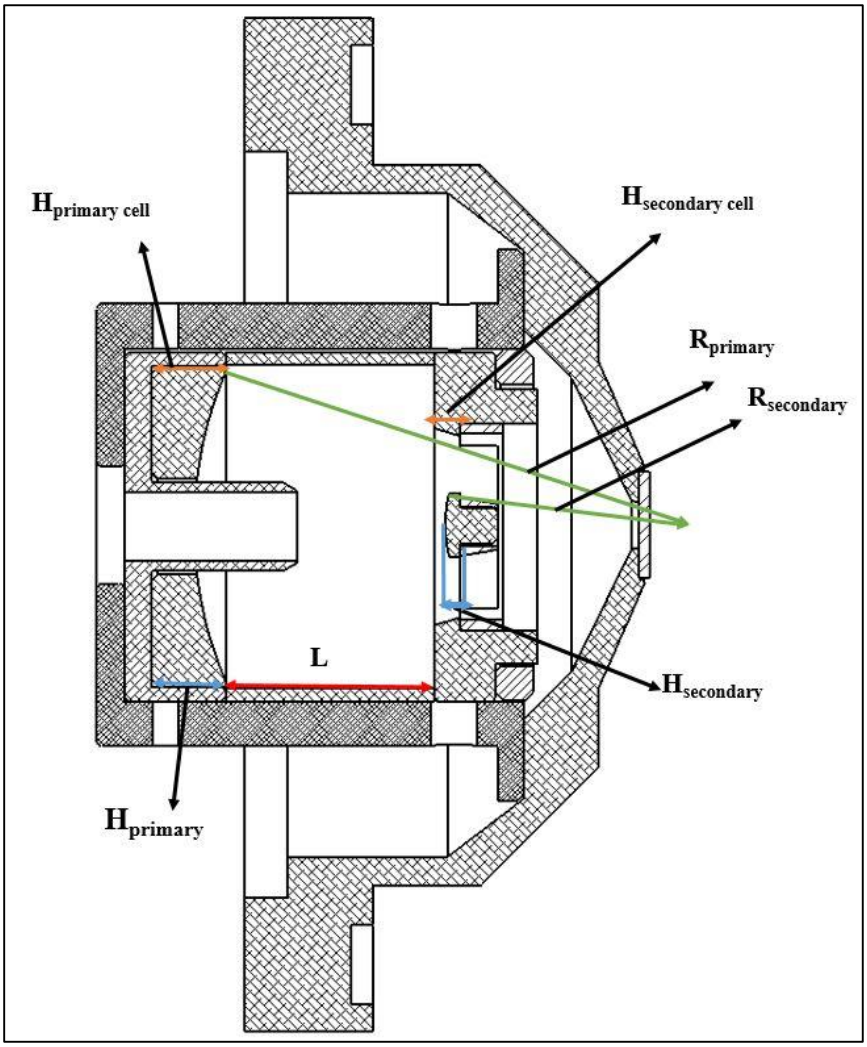

Fig. 26 Determine Spacer Thickness (L)

Table 6. Measured Parameters and Spacer Thickness (mm)

Parameter	Designed	Fabricated
H_Primary	8.98	8.979
H_Secondary	1.36	1.303
H_Secondary cell	2.5	2.497
H_Primary Cell	9	8.996
R_Primary	36.873	36.873
R_Secondary	12.6856	12.686
L		19.106

10.6 Window Mount/Vacuum Cap

The window mount/ Vacuum cap has two names, because the components have two primary purposes. The first purpose of the component is to mount the mirror. The LiF window mounts directly to a circular cut out region on the front surface of the window mount. A small amount of low outgassing two-part epoxy is carefully placed in the 25µm deep glue channels in the circular cut out region. The LiF window is carefully placed on the adhesive, and mild pressure is applied until the window sits flat on the mechanical mount. There are 4 mechanical glue dumps that are used to collect the excess glue when the LiF window is pressed into place. The barrel assembly attaches directly to the inside of the window mount using 8 radial tapped screw holes. The window mount can be attached and detached from the barrel assembly without affecting the alignment of the mirrors because of the compressive force from the retainer ring on the mirror cells.

The second purpose of the components is to allow the objective lens to attach to the microscope enclosure and hold vacuum pressure < 10^-3 torr. This portion of the component was designed to attach directly to a LF 63 6-way cross. To seal the vacuum, a Viton steel-centering ring is placed between the 6-way cross and the vacuum cap, as shown in Fig. 27.

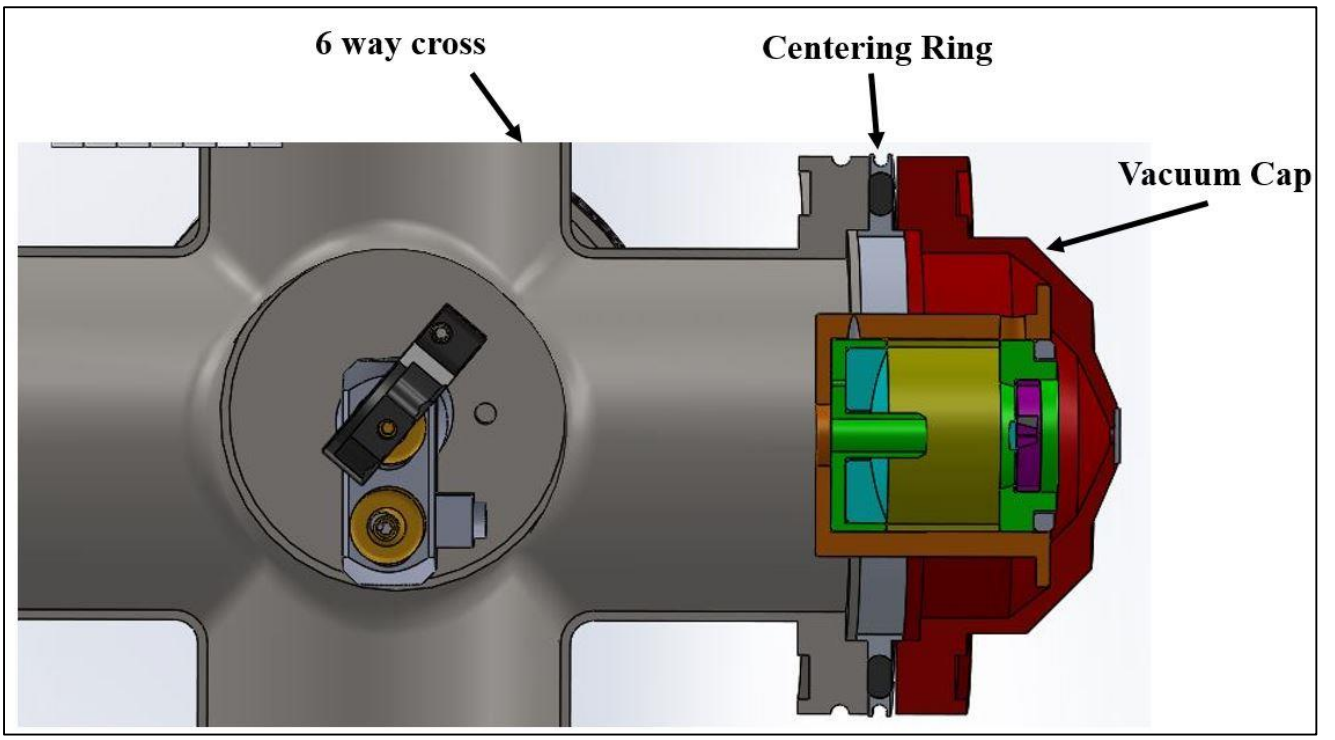

Fig. 27 Objective to LF 6-way cross

10.7 Retainer Ring

The retainer ring is designed to hold the assembled components inside of the barrel by applying a small compressive force to the stacked mechanical elements. The retainer ring is designed to slip over the outer diameter of the secondary cell. If the inner diameter of the retainer ring is not 0.5 mm greater than the outer diameter of the secondary cell, there is not enough compensation clearance for the adjustment of the secondary mirror decenter. The retainer ring over the secondary assembly is shown in Fig. 28.

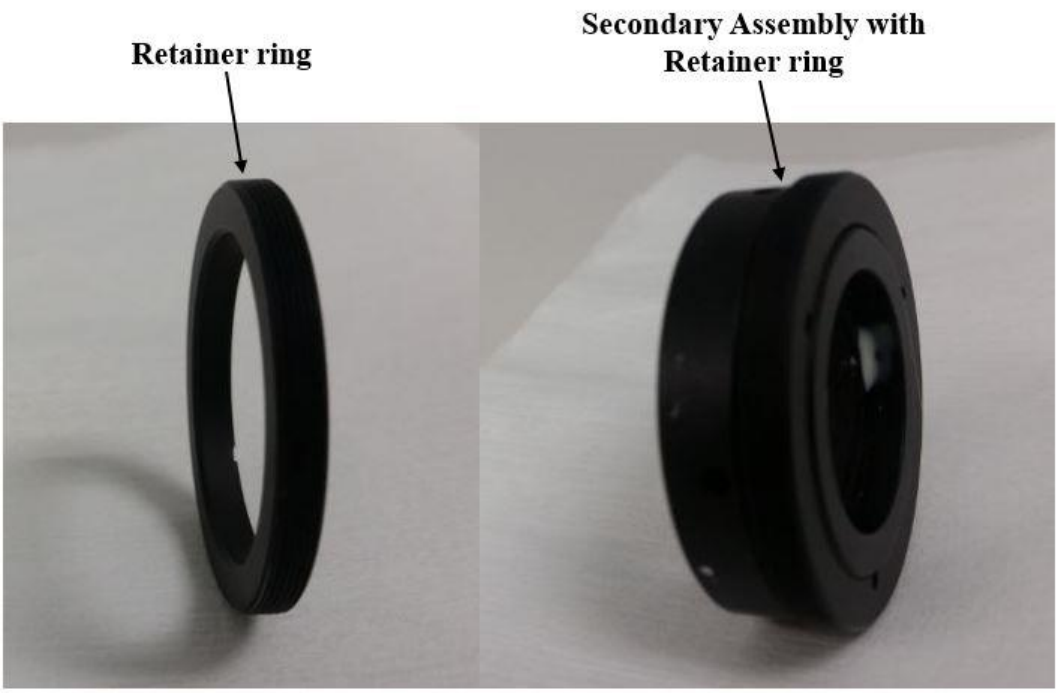

Fig. 28 (Left) Retainer ring (Right) Retainer with secondary assembly

10.8 Shim

The original designs of the primary and secondary mirrors were originally fabricated with thin thicknesses, which resulted in surface figure errors near the edges and thin sections of the components. Due to the surface figure errors, the mirrors are redesigned to be thicker. The primary mirror thickness is increased by 2 mm, and the secondary mirror thickness is increased by 1.3 mm. In order to use the same mechanics for the redesigned mirrors, a precision steel shim is added to the assembly. The shim is placed into the secondary assembly directly before the secondary spider.

11. Stray Light Control

The Andor Ikon-M SO is a low noise, high sensitivity camera; therefore, in order to obtain a high SNR of the sample image from our microscope the scattered light is minimized. There are two main sources of stray light: reflected light from the secondary mirror that does not propagate to the sample plane or directly to the CCD, and light that reflects from the secondary mirror and directly travels to the CCD. These sources of stray light are controlled separately.

The sources of stray light considered derive from the inherent design of a Schwarzschild Objective. In the imaging configuration there is loss of the central portion of the light that is blocked by the back aperture of the secondary mirror. This loss carries over into the illumination configuration, where the same portion of light is blocked by stray light controlling mechanisms. The HLA microscope utilizes a baffle, a circular aperture, and mechanical black paint to minimize the stray light.

The baffle is designed using a spread sheet that allows the user to vary the distance from the end of the baffle to the vertex of the secondary mirror. The optical design sets most of the parameters: V is the distance between the primary and secondary mirror vertices, θ_{inc} is the illumination light incident angle on the secondary mirror, θ_{cc} is the surface normal angle with respect to the incident light's radial location on the secondary mirror. The central portion of the secondary mirror that is obscured is defined by a 1.2 mm radial disk, and the baffle is designed such that the light reflected from this portion of

the secondary mirror is blocked by the baffle, and the remaining light is passed to the primary mirror. Figure 30 illustrates the necessity to block the central 1.2 mm radial disk on the secondary mirror. The black ray illustrates a ray that reflects right above the 1.2 mm region. The baffle does not block this ray and it will travel to the sample plane or the CCD camera. The ray in red illustrates the light from the sample that is blocked by the back of the secondary mirror. The blue ray illustrates a ray that is right below the 1.2 mm boundary. This ray is blocked by the baffle, but if it was not blocked the ray would clip the top surface of the secondary mirror and scatter into the objective assembly. The green ray illustrates a ray that is close to the optical axis. This ray is blocked by the circular aperture placed before the beam splitter, but it was not blocked the ray would contact the baffle and it would reflect back to the vacuum components and create a source of scatter. The baffle is designed with a fixed radius of BH = 4.125 mm. The incident ray angle is measured from the surface normal, and the law of reflection is used to determine the reflected ray angle. In the spread sheet, the designer places an arbitrary distance between the secondary mirror vertex and baffle edge, and determines the height of the reflected ray at that specific distance for the rays that are reflected from the various radial locations on the secondary mirror. If the height of the reflected ray minus the height of the baffle is greater than 0, then the ray is passed. If the height is less than 0, then the ray is blocked. The distance between the baffle edge and secondary mirror vertex is adjusted until the rays outside of the 1.2 mm radial disk are passed, and the rays inside the disk are blocked. The distance between the HLA microscope baffle and the secondary mirror vertex (FBL) is 15 mm. The baffle length

is 23.902 mm + 5.79 mm – 15 mm = 14.692 mm, which is shown in Fig. 31.

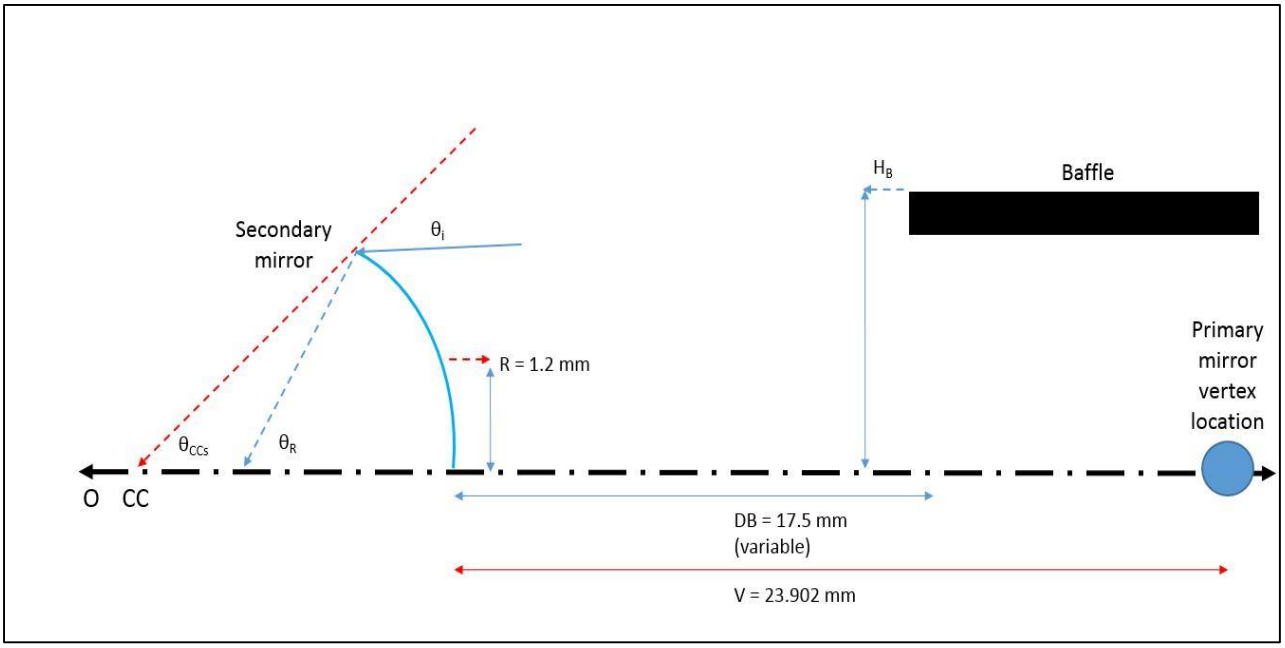

Fig. 29 Schematic for Baffle length calculation

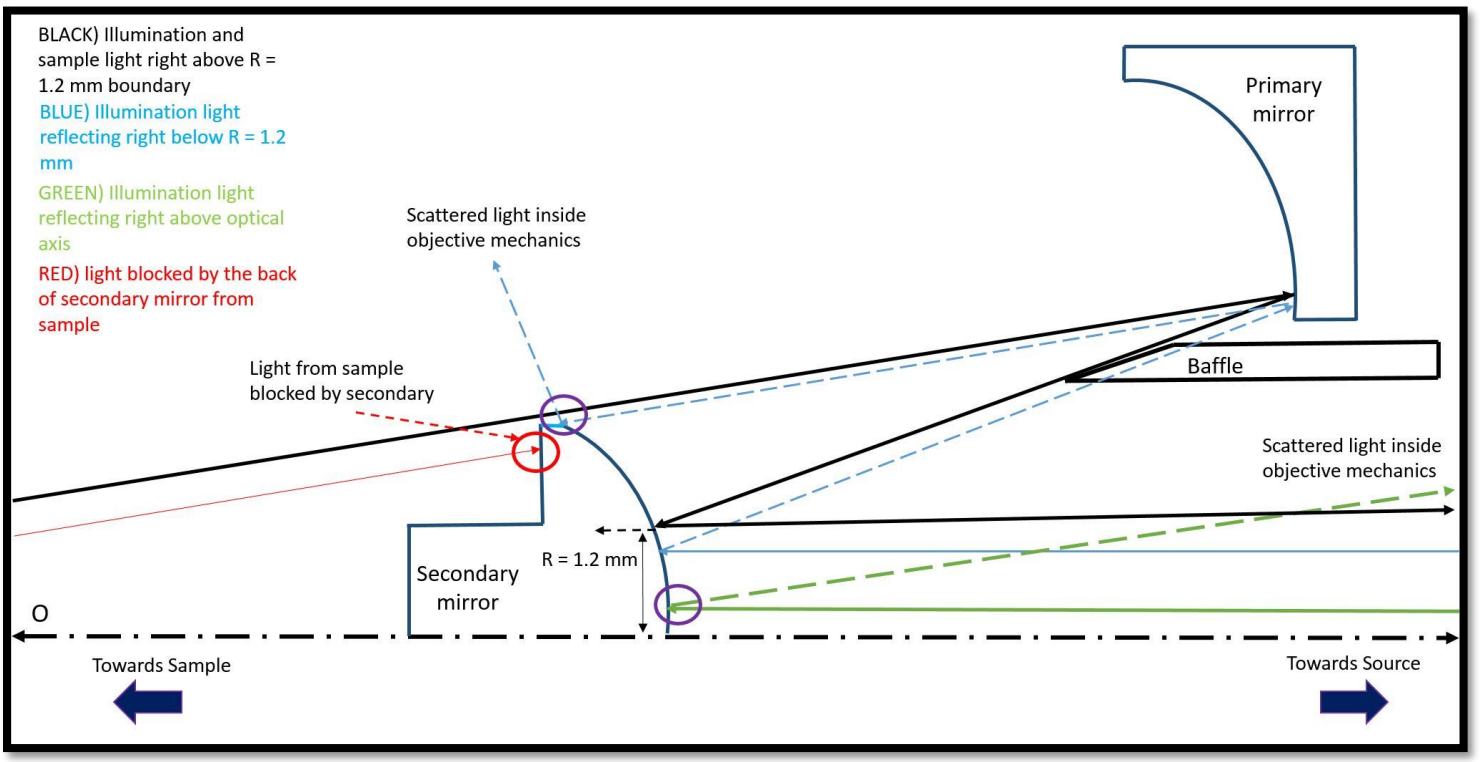

Fig. 30 Light reflecting from central 1.2 mm radial disk on secondary

Table 7. Baffle Design Table

RL	BH	ROC	Theta_cc	Theta_inc	Theta_refl	HB	Pass >0	FBL
3	4.125	12.6792	13.31	13.17	26.48	10.47	6.35	15
2.8			12.45	12.31	24.76	9.72	5.59	
2.6			11.59	11.44	23.03	8.98	4.85	
2.4			10.72	10.57	21.29	8.25	4.12	
2.2			9.84	9.70	19.54	7.52	3.40	
2			8.96	8.82	17.78	6.81	2.69	
1.8			8.08	7.93	16.01	6.11	1.98	
1.6			7.19	7.05	14.24	5.41	1.28	
1.4			6.30	6.16	12.46	4.71	0.59	
1.3			5.85	5.71	11.56	4.37	0.24	
1.2			5.41	5.26	10.67	4.03	-0.10	
1			4.51	4.36	8.87	3.34	-0.78	
0.8			3.61	3.47	7.08	2.66	-1.46	
0.6			2.71	2.56	5.27	1.98	-2.14	
0.4			1.81	1.66	3.47	1.31	-2.82	
0.2			0.90	0.76	1.66	0.64	-3.49	
0			0.00	-0.15	-0.15	-0.04	-4.16	

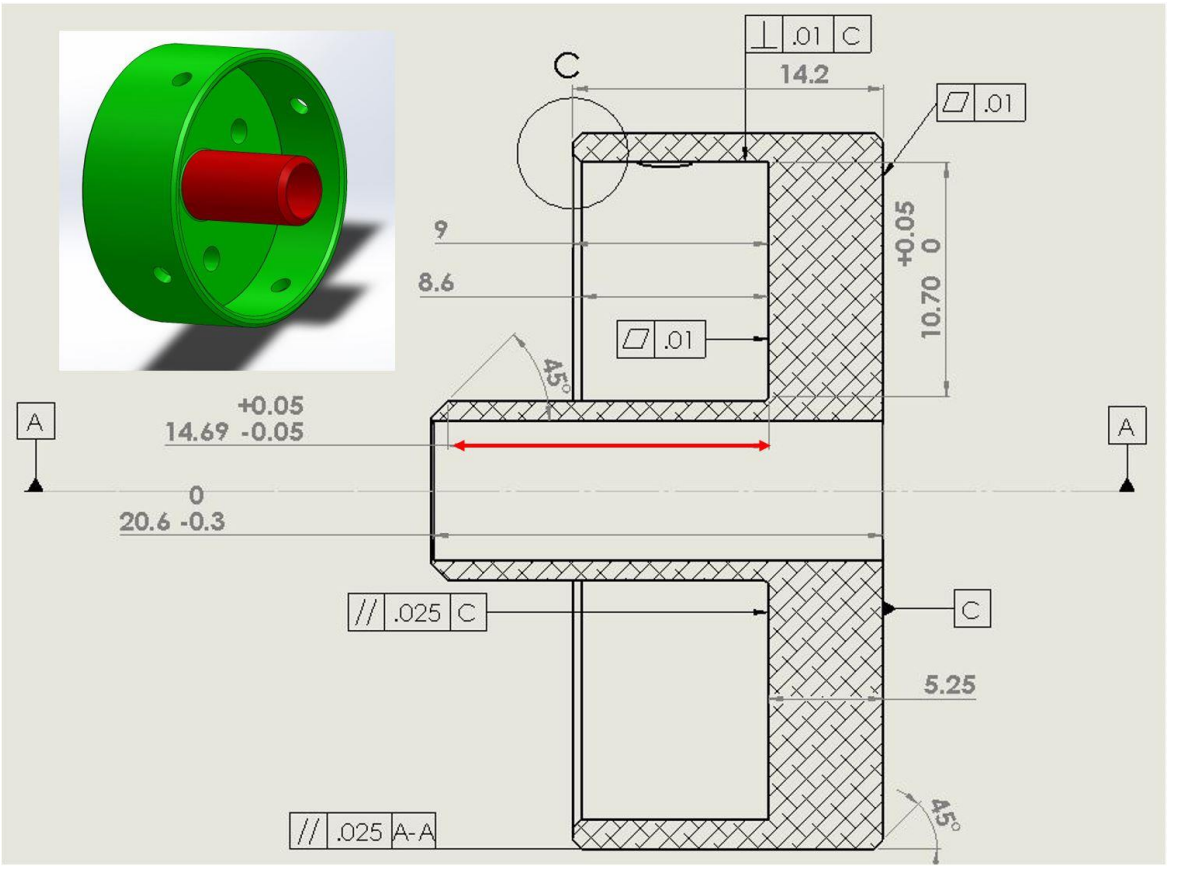

Fig. 31 Primary Mirror Cell and baffle drawing (Designed Baffle length in red)

The baffle stops all of the rays within the 1.2 mm disk from traveling to the primary mirror, but the baffle does not block the rays from the other mechanical components in the system. The baffle acts as a beam dump for rays greater than radial 0.85 mm to 1.2 mm central portion, but rays that are reflected from the secondary at a lower radial position than 0.85 mm will travel into the microscope chamber and potentially create a source of stray light. To minimize this stray light, a circular aperture placed 17 mm before the beam splitter blocks the illumination light and produces a shadow region on the central portion of the secondary mirror, which is shown in Fig. 32.

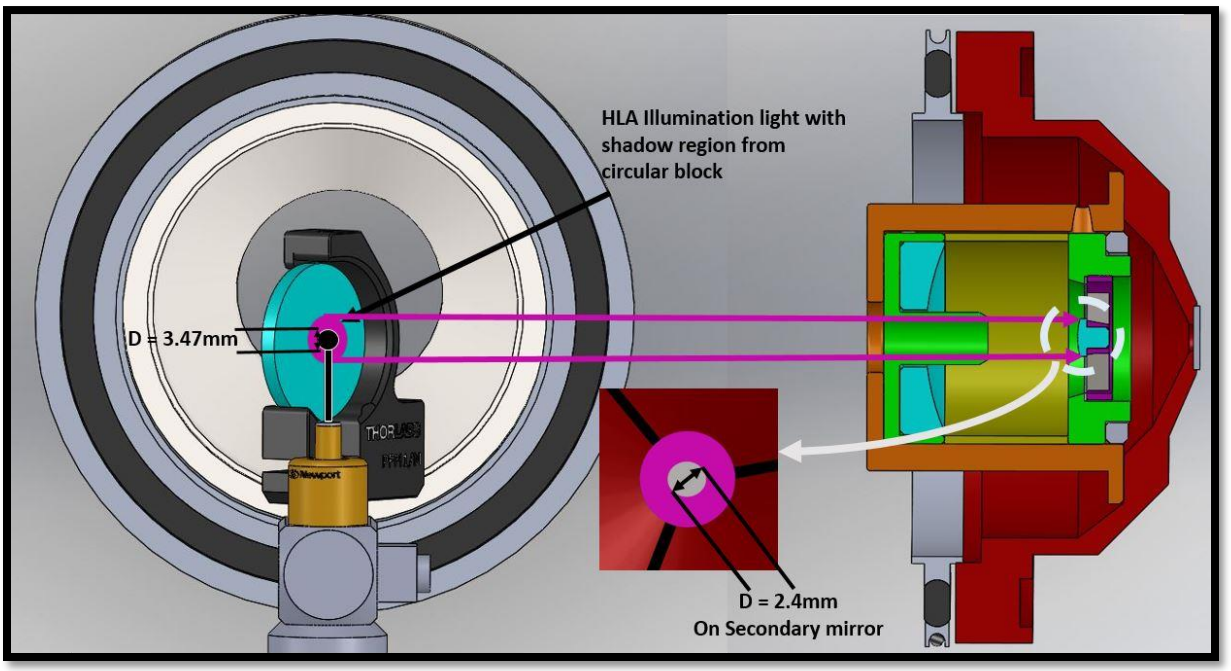

Fig. 32 Circular aperture before beam splitter is used to block light propagating towards the central portion (2.4 mm disk) of secondary mirror

The circular aperture is a 3D printed steel part that is glued into an optical post. The optical post sits inside of a custom right angle post sleeve that is attached to the beam splitter post. The alignment of the annulus is rough, and the shadow on the secondary may become elliptical or decentered. This alignment error causes a slight loss in throughput in the illumination configuration, and may also not eliminate the light on the entire radial 1.2 mm central disk. To ensure minimal stray light the inner surfaces of the HLA microscope are spray coated with Rustoleum flat black barbeque paint, which exhibits low outgassing, durable, high UV absorption. This coating is generally used in telescope baffling. [17][18].

12. Alignment

Ultraviolet optics are difficult to design and fabricate due to tight tolerances on optical and mechanical specifications. Generally, the tolerances are about five times tighter than visible optical systems due to the 5 times reduction in wavelength. An interferometer is a common instrument to test an optical system's performance, but most interferometers utilize visible wavelengths for testing. Therefore, an ultraviolet optical system's performance cannot be verified directly at the design wavelength by testing on an interferometer due to the reduction in fringe sensitivity. Alignment of the objective lens is achieved with a Point Source Microscope (PSM) on a Lens centering station (LCS) [15][16][17]. Alignment schematics are shown in Fig. 33. Alignment of the HLA objective system is performed using a PSM. A PSM is an advanced autostigmatic microscope that determines error in tilt and decenter. The PSM and rotary table combination allow for sub-micrometer correction of line of sight errors in a multi-element optical system [15][16][17]. The decentering tolerance of less than 1 μm is achieved in the alignment.

The HLA Objective lens assembly is a multistep process that is broken down into 3 main steps: cleaning, cell assembly, and point source microscope (PSM) on a lens centering stage (LCS) assembly.

12.1 Cleaning

All of the HLA objective lens components are thoroughly cleaned in order to reduce the amount of contamination. Contamination in ultra violet optical systems can greatly reduce transmission, and can also damage coating and reduce the lifetime of transmissive optical components [21]. The cleaning solvent of choice is acetone and high purity ethanol. The mirror surfaces are wiped with ethanol using a lint free cleanroom swab with very minimal force, and then quickly dried with nitrogen. The process is repeated until no residue can be seen on the surface of the mirrors. The mechanical components are placed in beakers of acetone and sonicated for 3 to 5 minutes. The components are then removed from the beakers, and then dried with nitrogen.

12.2 Cell Assembly

Once all of the optical and mechanical components are thoroughly cleaned, the mirror cells are assembled. A small amount of Hardman two part, urethane adhesive, Double Bubble is thoroughly mixed together. The primary mirror is carefully placed into the primary mirror cell. The primary mirror cell has 4 holes that are used for potting. A small toothpick-like object is used to place a very small amount of the adhesive inside each of the potting holes evenly such that the adhesive makes contact with the mirror outer wall and mirror cell inner wall. It is very important that the adhesive force at each of the hole locations is similar. The adhesive does not need to be placed around the entire edge of the potting hole; there only needs to be a small amount tacked onto a small area. Next, the secondary mirror is placed inside of the spider. The secondary

mirror and spider are carefully placed upside down with the center portion of the secondary mirror very lightly laying on top of a clean room swab. The mirror is then potted in place using the adhesive at 3 locations 120 degrees apart on the back beveled edge of the secondary mirror and the inner surface of the spider. The glue then hardens, which takes about 1 to 2 hours depending on how thoroughly mixed the two-part adhesive is. Once the adhesive has dried and the secondary mirror is securely placed into the spider mount, another small batch of the two-part adhesive is thoroughly mixed together. Then, the small shim is placed inside of the secondary mirror cell until it rests evenly on the inner lip. Then the spider is carefully placed in the secondary mirror cell until it rests on top of the shim. A small socket (from a socket wrench kit) is placed around the secondary mirror, such that it rests on the spider arms to ensure a good contact between the spider, shim, and secondary mirror cell lip by adding a small amount of force to push the components together. After the socket is carefully placed, a small amount of adhesive is added in 3 locations 120 degrees apart to the outer edge of the spider and the inner surface of the secondary mirror cell to keep the spider in place. Once the adhesive is applied, a LF or CF metal cap is balanced on top of the socket and the adhesive to dries for 2 to 3 hours.

Next, a small amount of the DUO Seal, UV, two-part epoxy is thoroughly mixed together. Then a small amount of the mixed epoxy is carefully placed 8 places (45 degrees apart) around the clear aperture of the window mount inside of the 25 μm deep trench. The LiF window is then gently placed on top of the aperture and fixed in place.

The residual epoxy will collect in the 4 outer collection trenches around the front extrusion of the window mount. To check if the window is vacuum sealed, the window mount is attached to the microscope enclosure, and is pumped down. If the system is not pumping down, or if the system is not maintaining pressure, then the window is not sealed correctly.

12.3 Barrel Assembly on LCS

The LCS and PSM alignment theory is described above. In order to effectively achieve the specified centering alignment tolerance of ±1 μm on LCS, the procedure below is followed. The LCS at the College of Optical Sciences is equipped with a x-y-z translation mount, tip-tilt mount, and a circular base plate with adjustment screw placement holes. There are three 100 thread per inch adjustment screws that are placed 120 degrees apart on the top plate used to adjust the primary mirror. The top mounting plate has a through hole that is close to concentric with the outer diameter of the plate. The summarized alignment procedure is shown in in Table 8.

The PSM is equipped with a LED and a laser diode. A 10X Nikon objective is attached to the PSM. The tube lens has a length of 100mm, which reduces the real magnification of the system to 5X instead of 10X. With the reduction each pixel corresponds to 0.75μm /pixel. The pixel size on PSM CCD (FL2G-13S2M-C) is 3.75 μm; therefore, each pixel corresponds to 0.75μm.

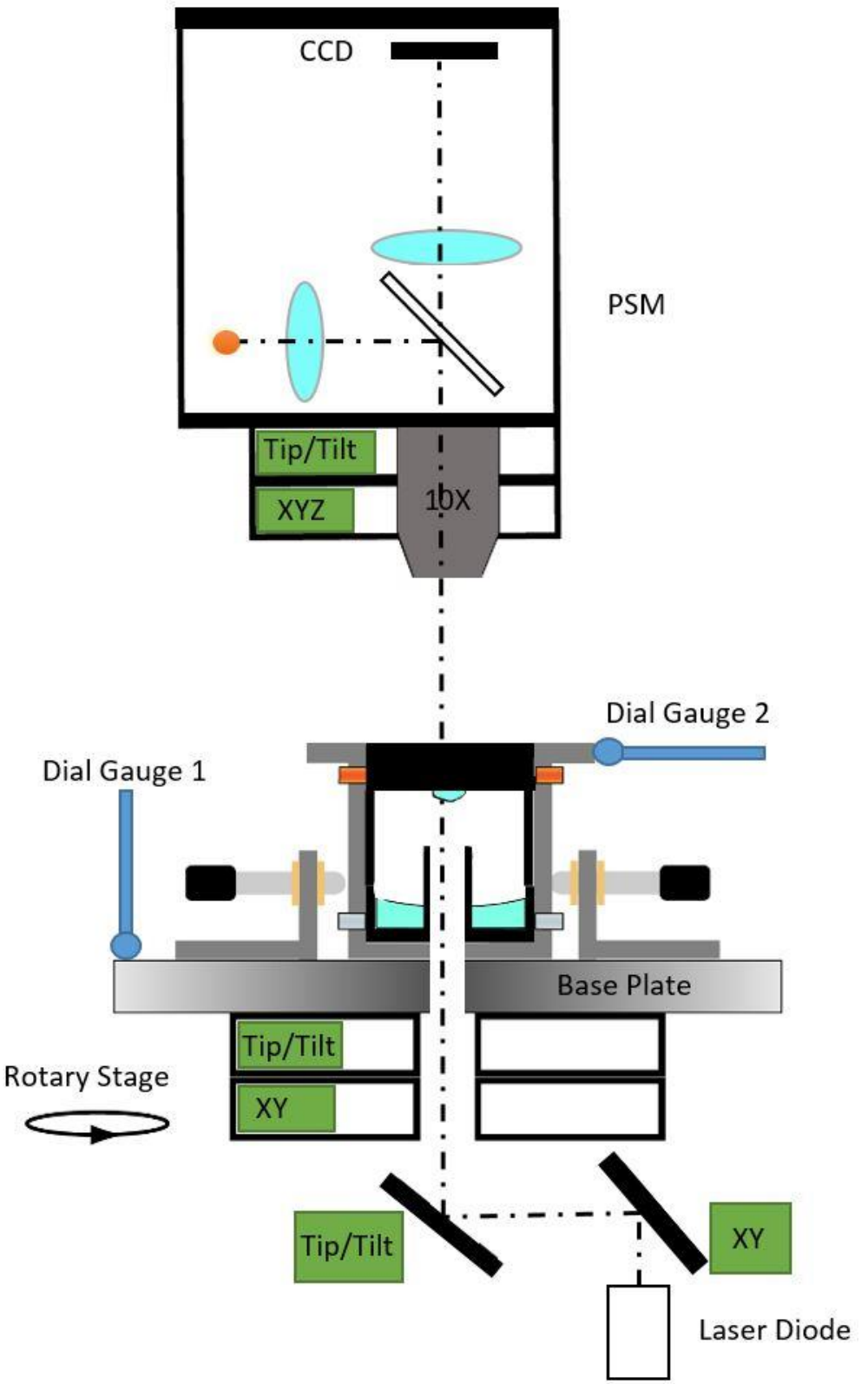

Fig. 33 PSM/LCS Full Alignment schematic

Table 8. Alignment on LCS

Steps	Action	Purpose
0	Use Corner cube to set reference position on PSM CCD (no mechanical adjustment needed)	Set reference point on CCD
1	Align normal of baseplate w/ mechanical axis dial gauge on the base plate (stage tip/tilt) Align Barrel centering w\ dial gauge on the outside of barrel (stage x/y) Roughly Align PSM collimated beam (PSM x/y)	Normal of base plate aligned to mechanical axis of rotation Centering of barrel roughly align PSM axis
2	Place parallel flat inside barrel and with collimated beam from PSM. Use stage (tip/tilt) to minimize radial trajectory of reflected spot around reference point from step 0	Normal of flat aligned to mechanical axis of rotation
3	Adjust PSM (tip/tilt) until the reflected spot on CCD coincides w/ reference from step 0	PSM axis aligned to mechanical axis of rotation
4	Place an object with suitable height inside of barrel (grating on platform is good). Use PSM LED to image top surface of grating onto CCD. Adjust PSM (x/y) until axis of rotation of grating coincides with reference from step 0	Centering PSM (x/y)
5	Turn on Laser Diode (LD). Use two mirror (x/y/tip/tilt) to align LD spot with reference point from step 0	LD axis aligned to PSM axis
6	Repeat steps 4-5 until PSM axis coincides with mechanical axis of rotation: Align PSM with a rough surface Align PSM with LD (PSM t/t) Iterate until spot is stationary w/ and w/o objective	PSM centering PSM axis w/ LD axis PSM axis coincide w/ mechanical axis

7	Place Primary mirror cell into barrel and fix with adjustment screws	Primary centering
8	Insert spacer and secondary mirror cell. Use LD and move z axis of PSM to image the infinite conjugate position. Align secondary mirror using adjustment screws. Thread in retainer ring.	Objective Alignment

13. Summary and Next Steps

The VUV microscope described in this thesis presents unique optical and mechanical engineering problems. There is limited availability of materials that transmit in the UV, so the majority of the optical components in the system are reflective. The materials that transmit in the VUV are LiF and MgF2, but due to unwanted polarization effects in MgF2 LiF is used as the window of the objective lens. UV optics are difficult to design and fabricate due to the tight tolerances at this wavelength. The optical tolerances in the UV are roughly 5 times tighter than optical systems in the visible. Also, the optical performance of the objective lens at the design wavelength is not able to be interferometrically determined because of the reduction in fringe sensitivity of visible interferometers. Outcomes from this research are the design of an optomechanical objective lens capable of achieving the tight tolerances necessary for diffraction limited performance in the VUV, a optomechanical design and layout of the critical illumination setup inside of the microscope vacuum enclosure, and an alignment procedure for aligning the objective lens on a lens centering stage. The information presented in this this thesis lays the foundation for future development of the HLA microscope.

As expected, the fabrication of the optical and mechanical components proved to be difficult. The first iteration of the primary mirror was fabricated with a surface figure error out of tolerance. The exact reason for the fabrication error is unknown, but an idea is that the error is due to the inner thickness of the primary mirror is too thin. In order

to correct this error, a second primary mirror is currently being fabricated with a 2mm increase in thickness. Another major fabrication error is the outer diameter of the primary mirror cell is larger than the maximum allowable tolerance. This fabrication error does not allow the primary mirror to be centered inside of the barrel during the alignment procedure. A new primary mirror and primary mirror cell are being fabricated to correct for these errors. The revision tables of the optomechanical components are shown in the Appendix C. Once the new parts are fabricated, the next steps are to align and test the objective lens, then attach the objective lens to the microscope enclosure and begin taking images in VUV.

Appendix A

Gas Manifold Gauge Calibration

Gauge Reading	Stinger reading(Torr)
0	752
2	715
4	670
6	619
8	555
10	497
12	444
14	393
16	340
18	283
20	221
22	181
24	136

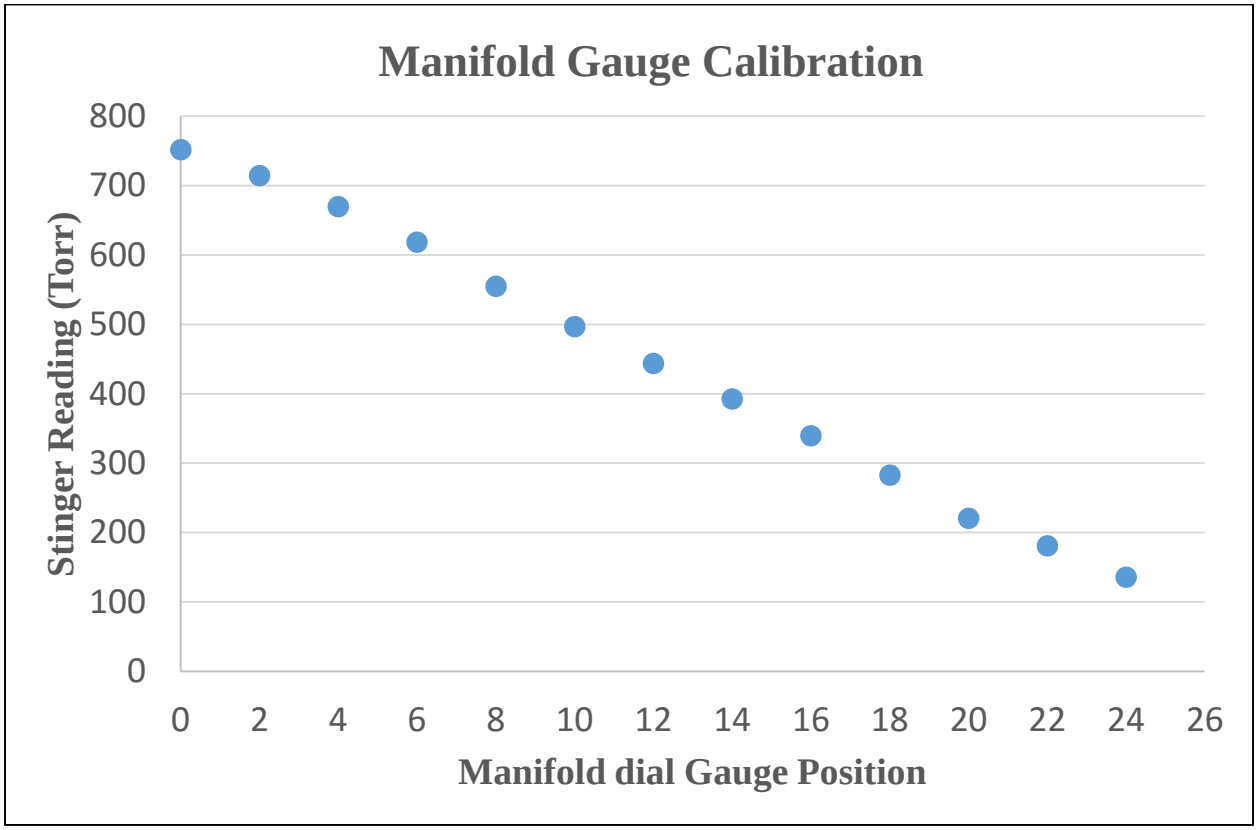

Lamp Lighting Procedure

1- Close all of the shut off valves (V1, V2, V3, and V4), leave NV or flow control open to near maximum flow.
2- Turn the manifold pump ON.
3- Open V3 until you reach the ultimate pressure of the pump (let run for 5 minutes).
4- Open V2 SLOWLY.
5- Open V1. 6- Evacuate the system until you reach the ultimate pressure of the system (Let run for 5-10 minutes).
6- Close V3 and V2 to ensure that the system is leak tight. (this step is only necessary if the system has not been used in a while, or if the source is not lighting).
7- Make sure gas regulator pressure is less than 0.5 atmosphere (7.5 psi).
8- Flush the lamp by slowly opening V4 to fill lamp to about 200 torr, then close V4 and pump out again. Repeat this step at least twice.
9- Evacuate until you reach the ultimate pressure of the pump.
10- Close the NV.
11- Open V4 SLOWLY to fill the lamp with the gas mixture until the pressure gauge reads about 175 to 200 torr. Then close V4
12- The Lamp is now ready for operation
13- The BNC cables should already be connected to the lamp
14- The Power supply should already be set up with the correct frequency (highest) and pulse width (set to max)
15- Turn on the high voltage
16- If the source does not light within 10-20 seconds, then slowly lower the pressure in the lamp by SLOWLY opening the needle valve. Do not let the pressure fall below the 24 (136 torr).
17- Once the lamp lights, open V4 until the pressure is set for maximum 121.6 nm output.
18- Close V4 slightly, and open NV slightly such that there is a minimal flow of the gas mixture through the lamp. DO NOT WASTE GAS BY HAVING TOO HIGH OF A FLOW!

Appendix B

Mechanical Revision Tables

Table 9. Mechanical Revision Table

Primary Mirror	1	5/20/2015	• Iteration 1
	2	6/30/2015	• Reduced tolerances on non-critical dimensions
	3	1/5/2016	• Mirror height increased by 2mm in order to reduce surface figure error during fabrication
Secondary Mirror	1	5/20/2015	• Iteration 1
	2	6/30/2015	• removed the center through hole • added a chamfer to back surface to be used as a glue channel
	3	8/20/2015	• Secondary Mirror height was increased by 2mm in order to reduce surface figure error

Table 10. Primary Mirror Cell Revision Table

PART	REVISION	DATE	• CHANGES/REASON
Primary Cell	1	5/20/2015	• Iteration 1
	2	6/30/2015	• Reduced tolerances on non-critical dimensions to reduce cost
	3	7/29/2015	• Added 3 (Q) holes on the back surface in order to help with the removal of the primary mirror • Added datum surface C in order to clearly specify the reference surface
	4	8/20/2015	• Decreased the clearance for the primary mirror to 50 micrometers • Increased the baffle length to reduce stray light from secondary mirror • Increased the baffle ID to eliminate vignetting in the illumination path
	5	1/5/2016	• Increased the Q holes to 2mm from 1mm to make primary mirror removal easier • Optimized the baffle length to 12.19mm with a 2mm thicker primary mirror

			• Increased the cell height by 2mm in order to accommodate for the increase of the primary mirror thickness

Table 11. Secondary Spider Revision Table

PART	REVISION	DATE	CHANGES/REASON
Secondary Spider	1	5/20/2015	• Iteration 1
	2	6/30/2015	• removed potting holes for the secondary mirror and added a bevel surface to the back of the secondary mirror • Reduced the tolerance on spider arm thickness to reduce cost

Table 12. Secondary Cell Revision Table

PART	REVISION	DATE	CHANGES/REASON
Secondary Cell	1	5/20/2015	• Iteration 1
	2	7/29/2015	• Increased the inner diameter of the aperture by 10% as a safety factor in order to eliminate vignetting
	3	8/20/2015	• Designed a cut out slot to fit the retainer ring over the secondary cell

Table 13. Objective Barrel Revision Table

PART	REVISION	DATE	CHANGES/REASON
BARREL	1	5/20/2015	• Iteration 1
	2	6/30/2015	• Added 6 -M3-0.5 D.P 3.2 callouts to attach the barrel onto the tooling base plate • Reduced tolerances on non-critical dimensions • Changed secondary mirror adjustment screws to M4x0.7
	3	7/29/2015	• Increased entrance aperture of barrel to 11mm • Changed secondary mirror adjustment screws to M4.5x0.7
	4	8/20/2015	• Increased total length of barrel by 1mm

			• Added M33x0.5 internal thread for a retainer ring
	5	1/5/2016	• Primary mirror adjustment screws changed to press fit bushing holes (same as secondary adjustment screws • Reduce the number of adjustment holes for the PMC to 3 • Increased ID of barrel by 0.2mm for more compensation • Added datum surface B and reference alignment tolerances on surfaces that will be used during alignment with dial indicators • Increased length of the barrel in order to fit new PMC with existing spacer • Added features to allow for flush fitting of the adjustment screws bushing, this was recommended by KBSI • Increased the tap length of the retainer ring thread

Table 14. Spacer Revision Table

PART	REVISION	DATE	CHANGES/REASON
Spacer	1	5/20/2015	• Iteration 1

Table 15. Vacuum Cap/ Window Mount Revision Table

PART	REVISION	DATE	CHANGES/REASON
Vacuum Cap	1	5/20/2015	• Iteration 1
	2	7/29/2015	• Increased clear aperture to allow for 10% error in order to eliminate any vignetting
	3	8/20/2015	• Optimized the thickness of the window mount for an increased thickness change of the secondary mirror

Table 16. Retainer ring Revision Table

PART	REVISION	DATE	CHANGES/REASON
Retainer Ring	1	8/20/2015	• In order to maintain compressive force on the mirror cells, and to allow the vacuum cap to be assembled and disassembled without affecting the alignment a retainer ring is added that screws into the barrel and contacts the secondary cell

Table 17. Shim Revision Table

PART	REVISION	DATE	CHANGES/REASON
Shim	1	1/5/2015	• Added shim between secondary cell and secondary spider due to primary mirror increased thickness and fabricated spacer thickness

Appendix C

HLA Objective Lens Assembly Drawing

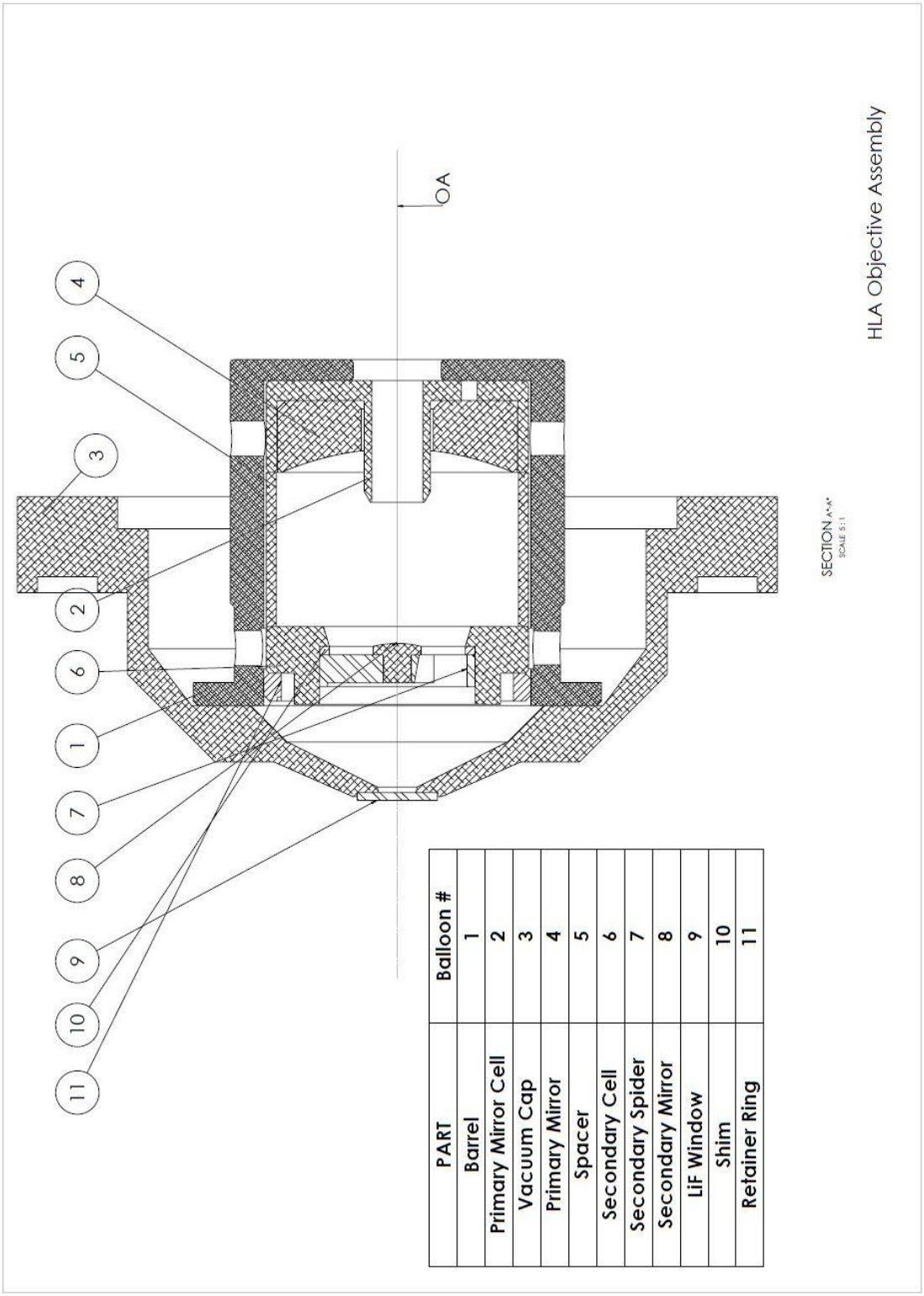

PART	Balloon #
Barrel	1
Primary Mirror Cell	2
Vacuum Cap	3
Primary Mirror	4
Spacer	5
Secondary Cell	6
Secondary Spider	7
Secondary Mirror	8
LiF Window	9
Shim	10
Retainer Ring	11

Barrel Drawing

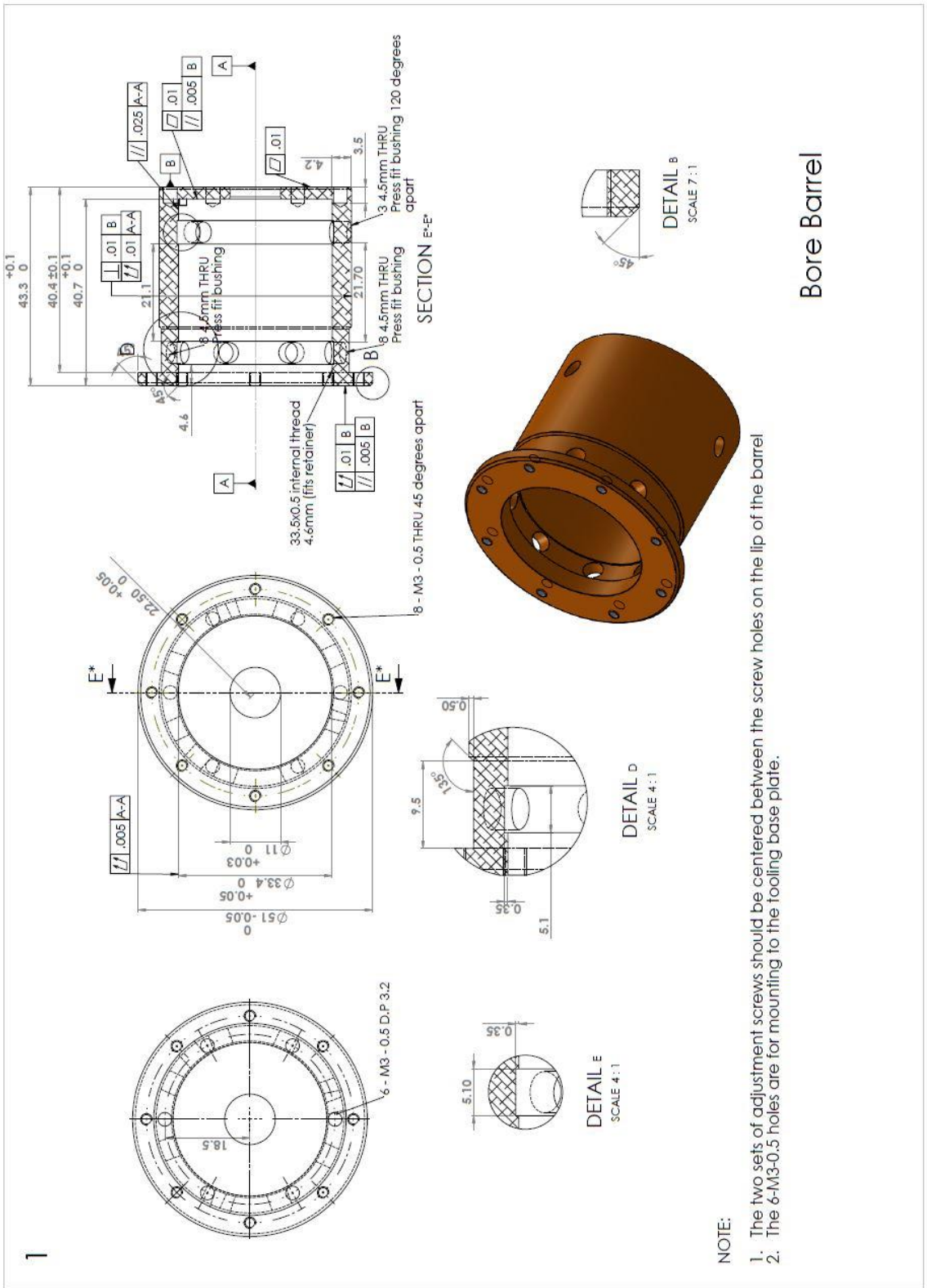

Primary Mirror Cell Drawing

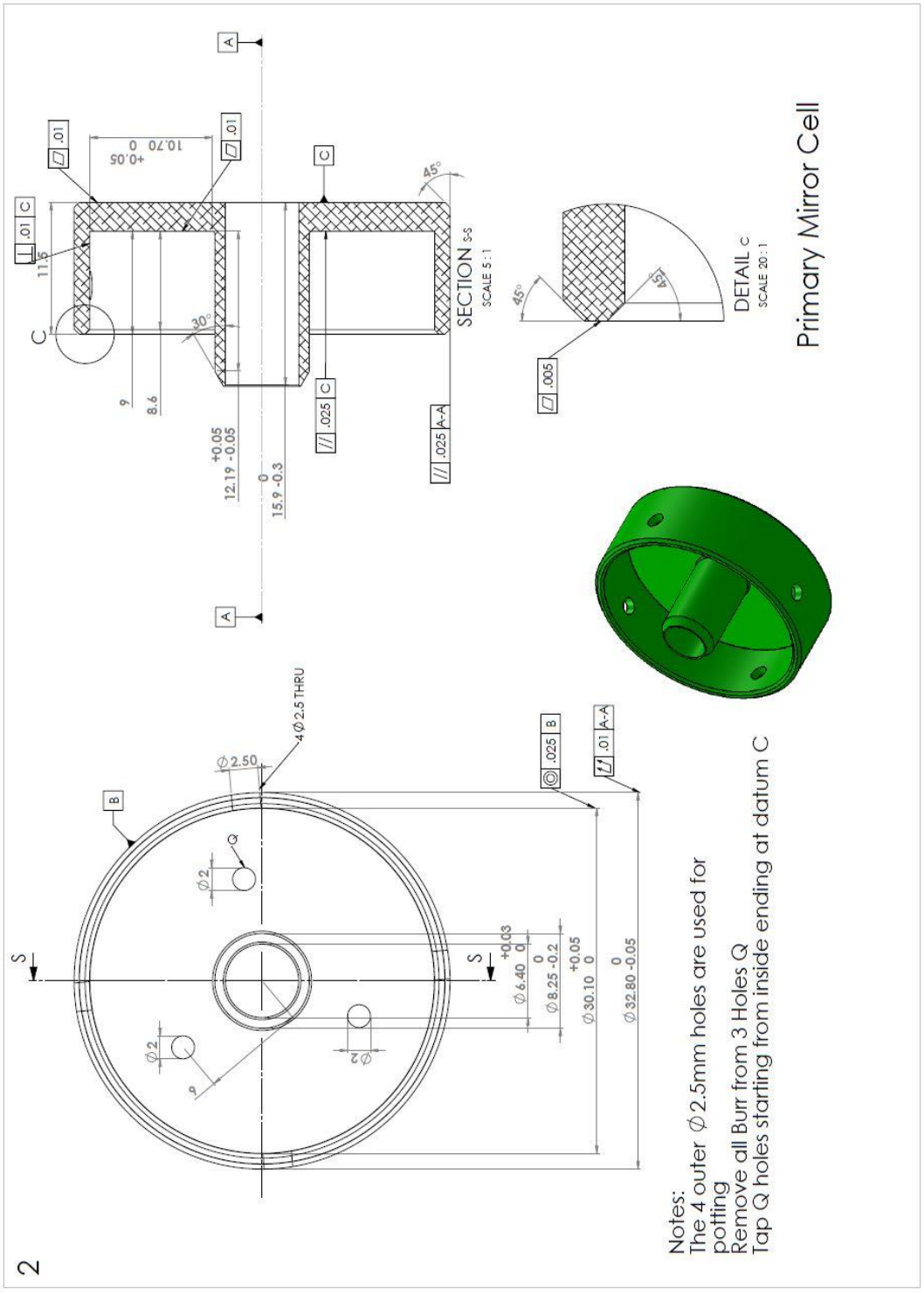

Updated Primary Mirror Cell Drawing

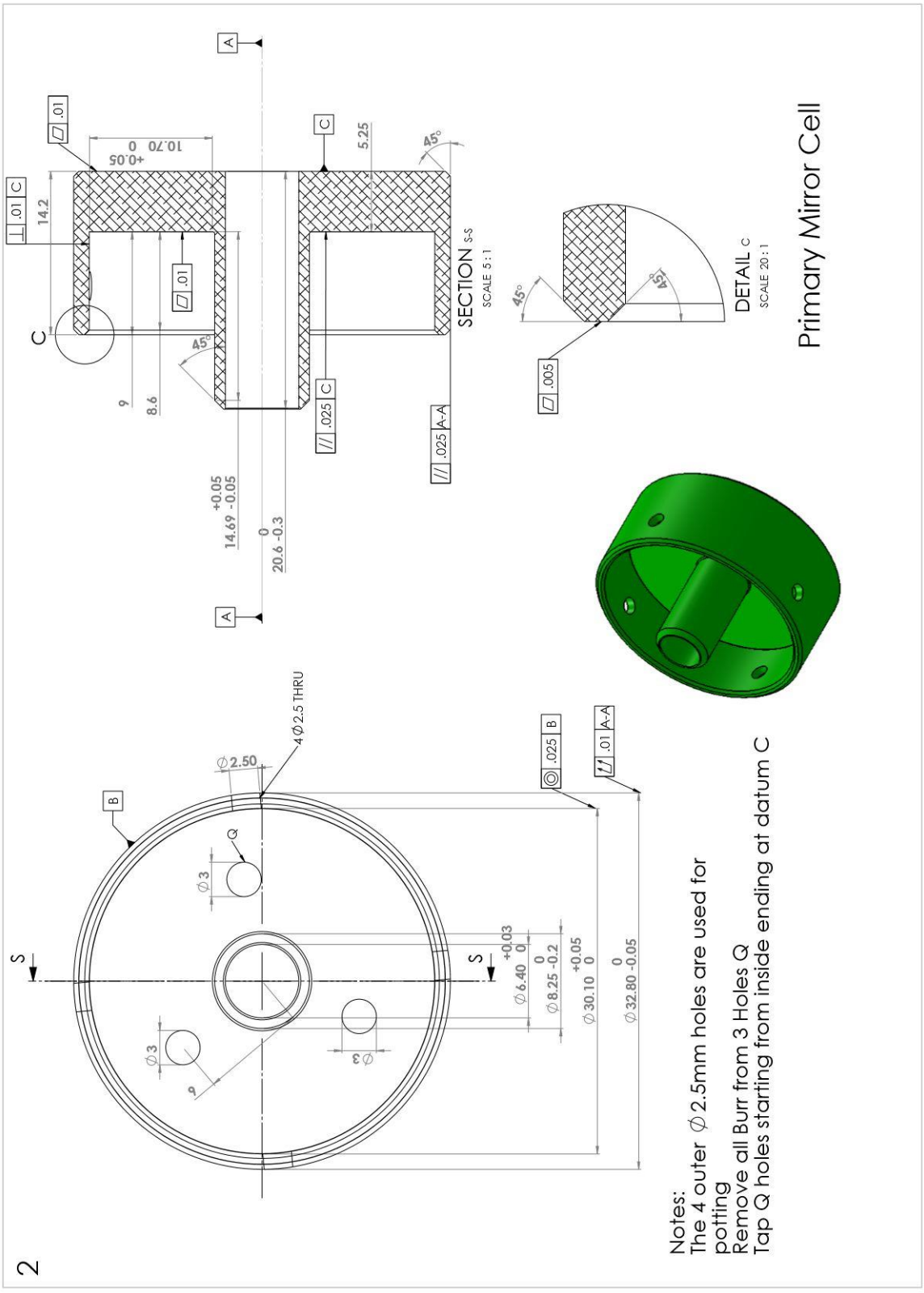

Vacuum Cap Drawing 1

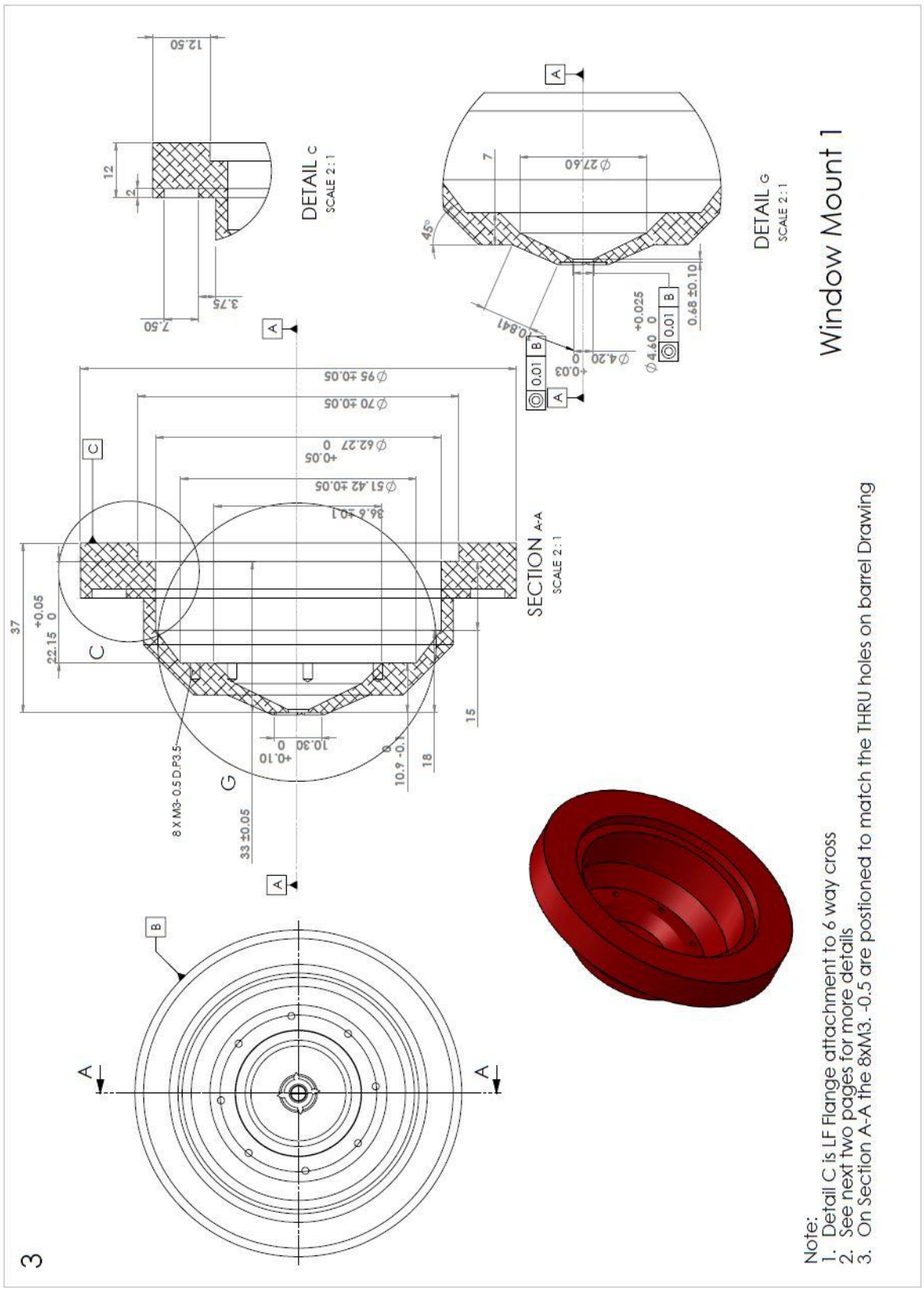

Vacuum Cap Drawing 2

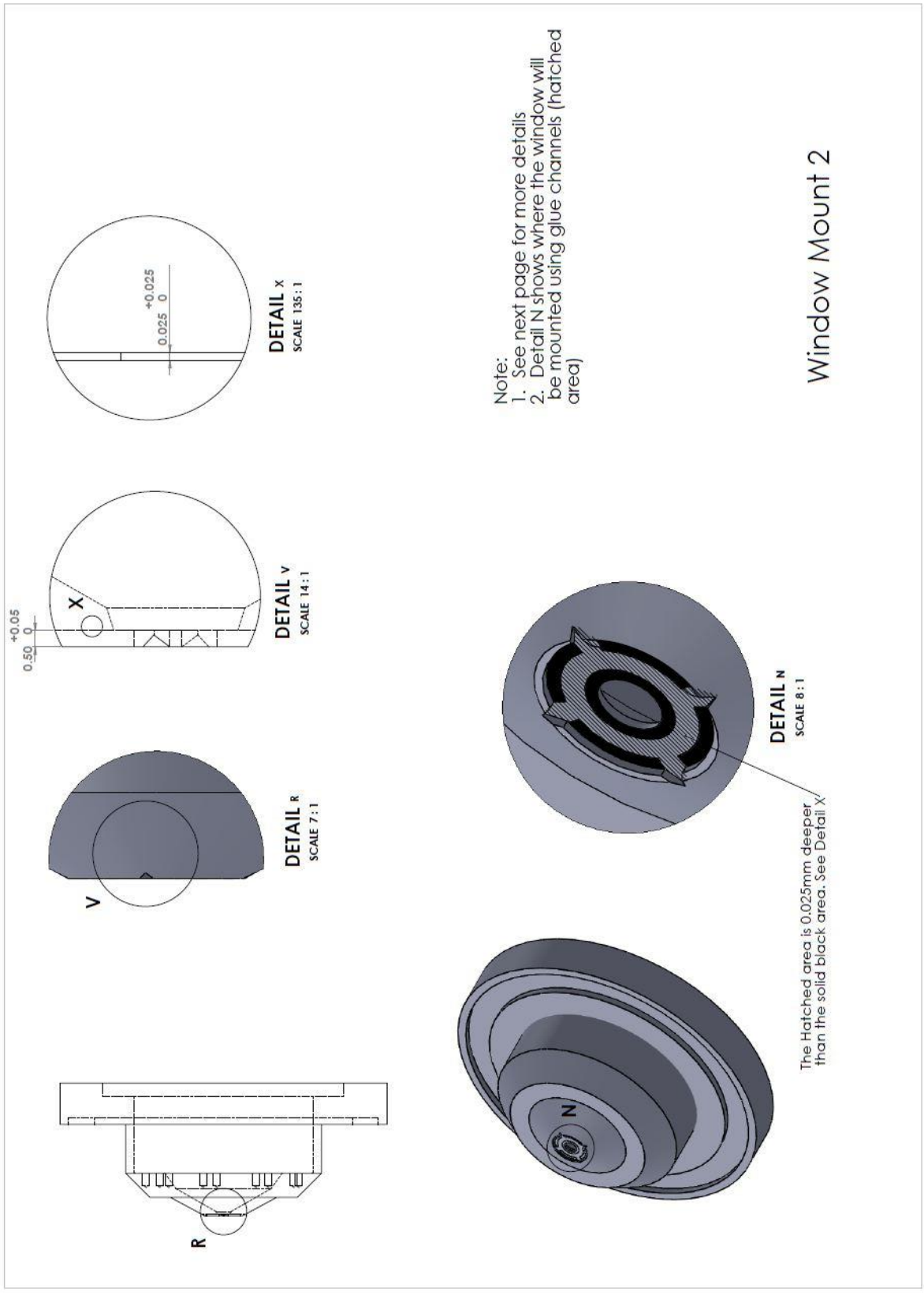

Vacuum Cap Drawing 3

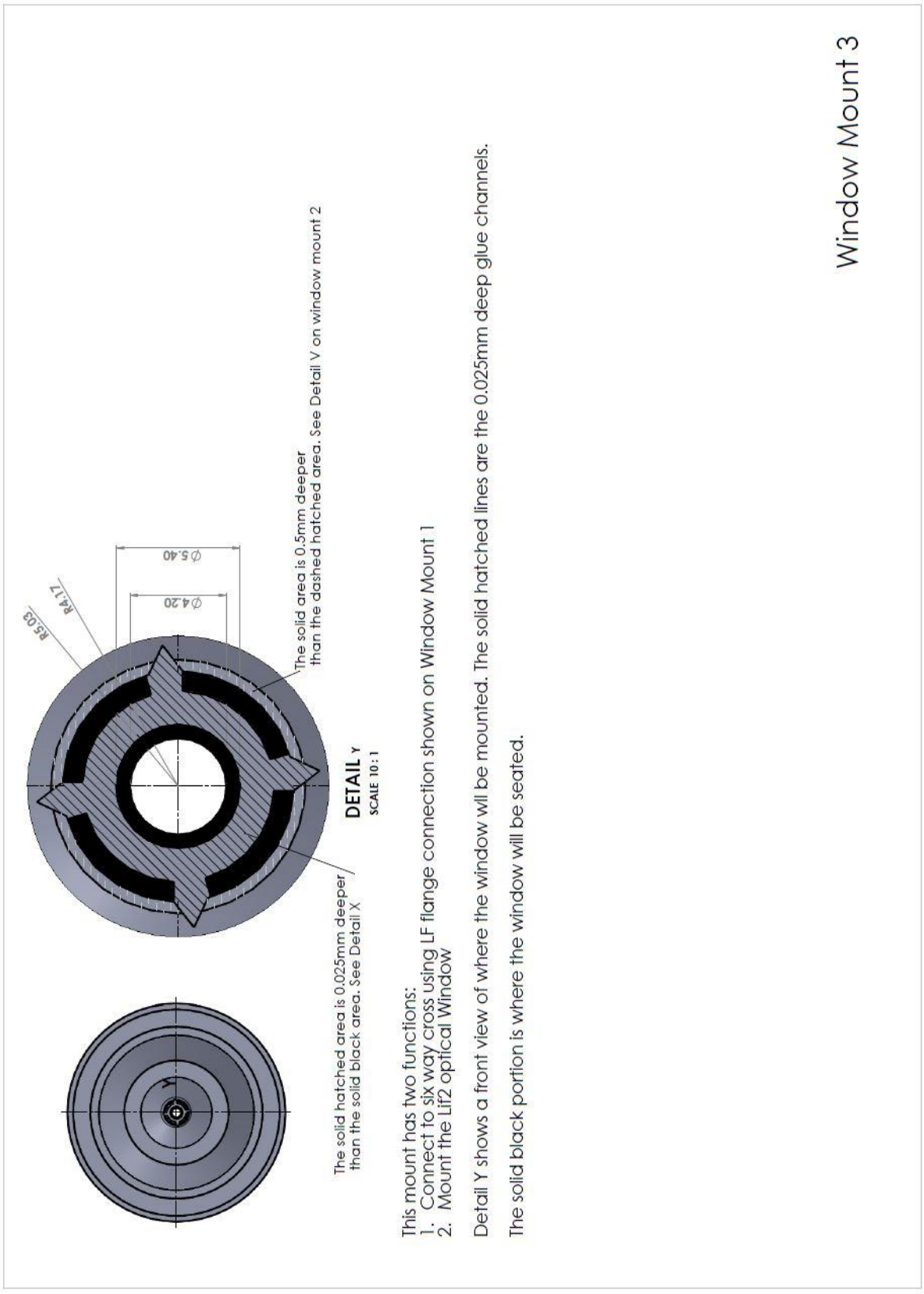

Primary Mirror Drawing

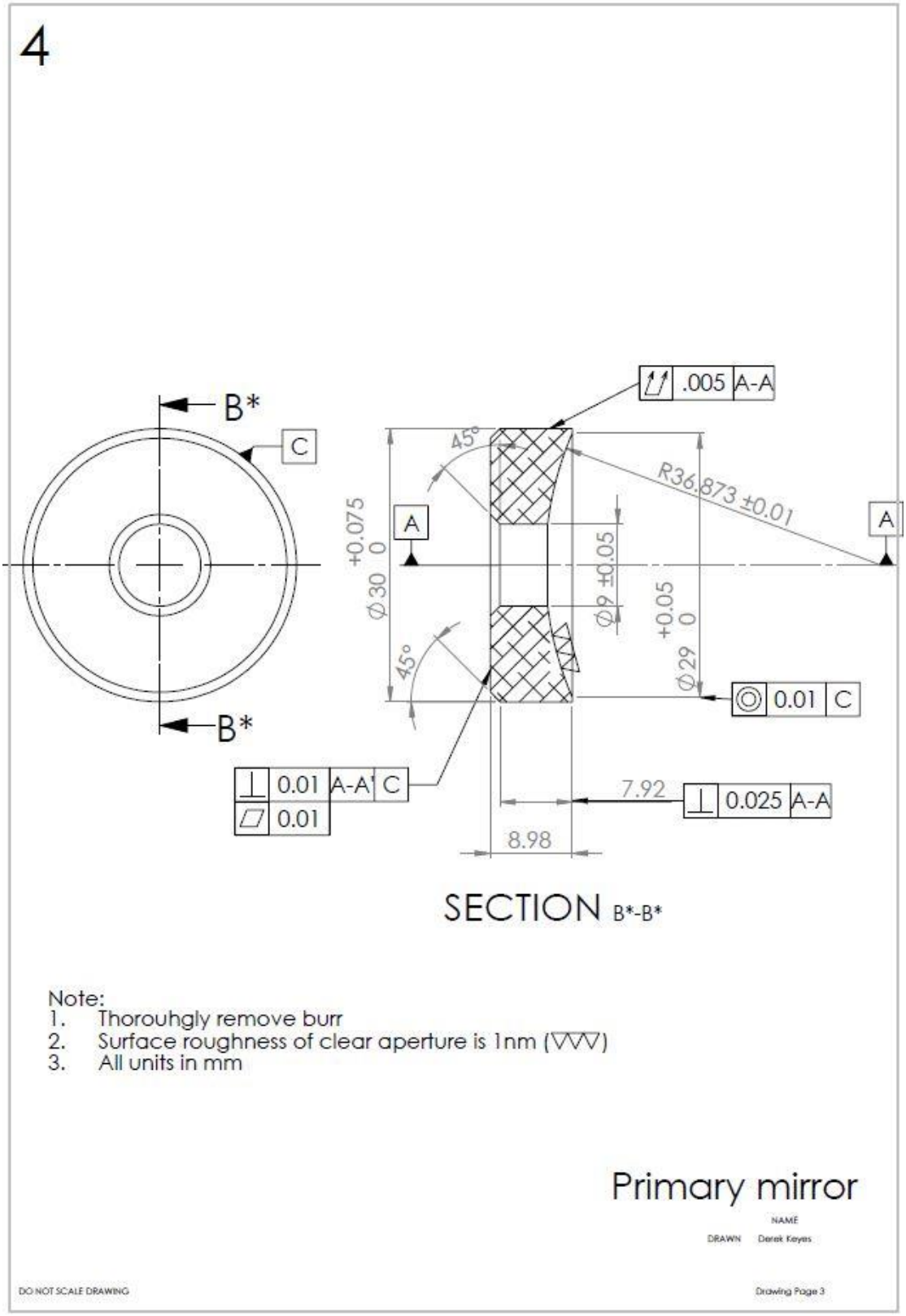

Spacer Drawing

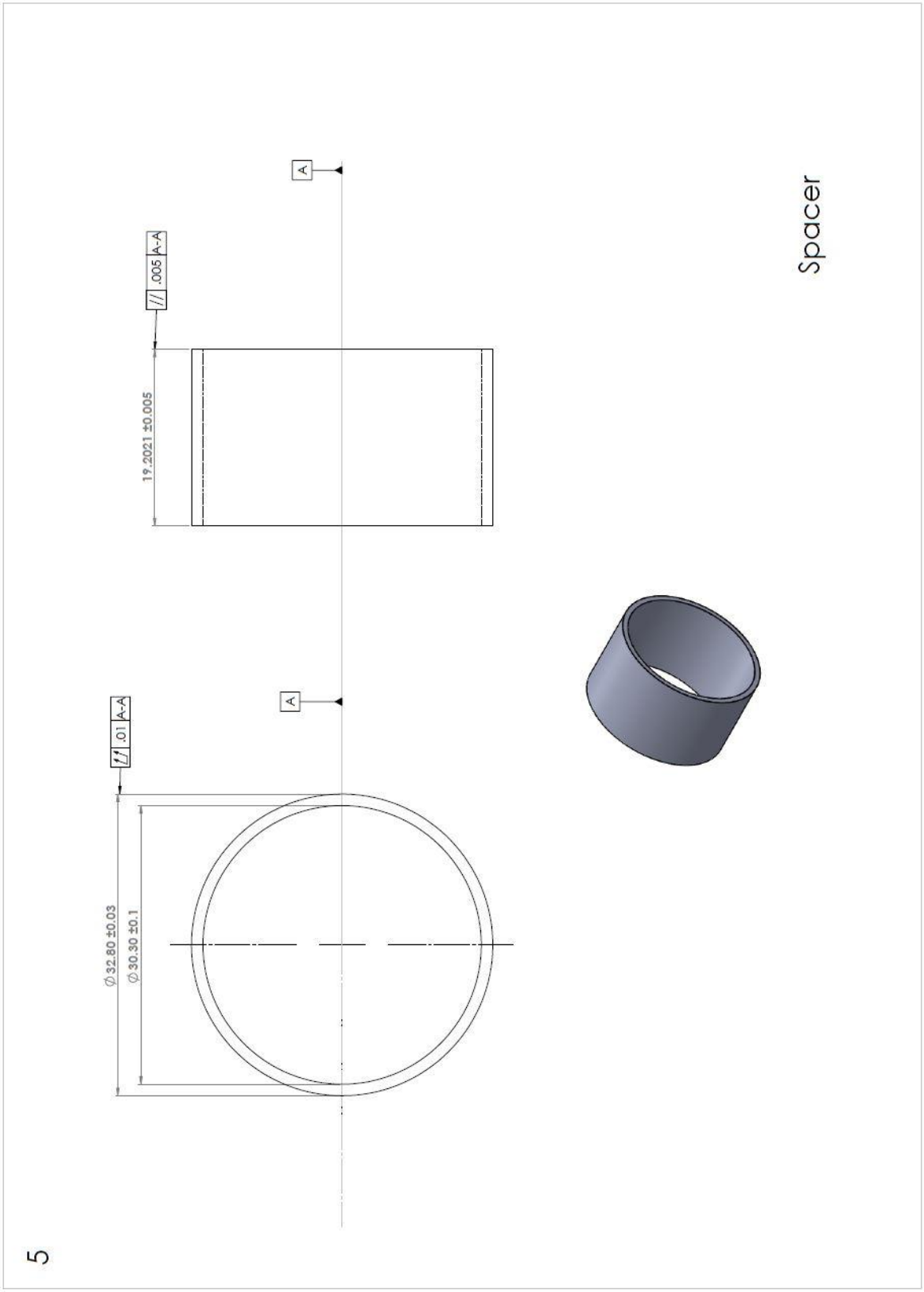

Secondary Cell Drawing

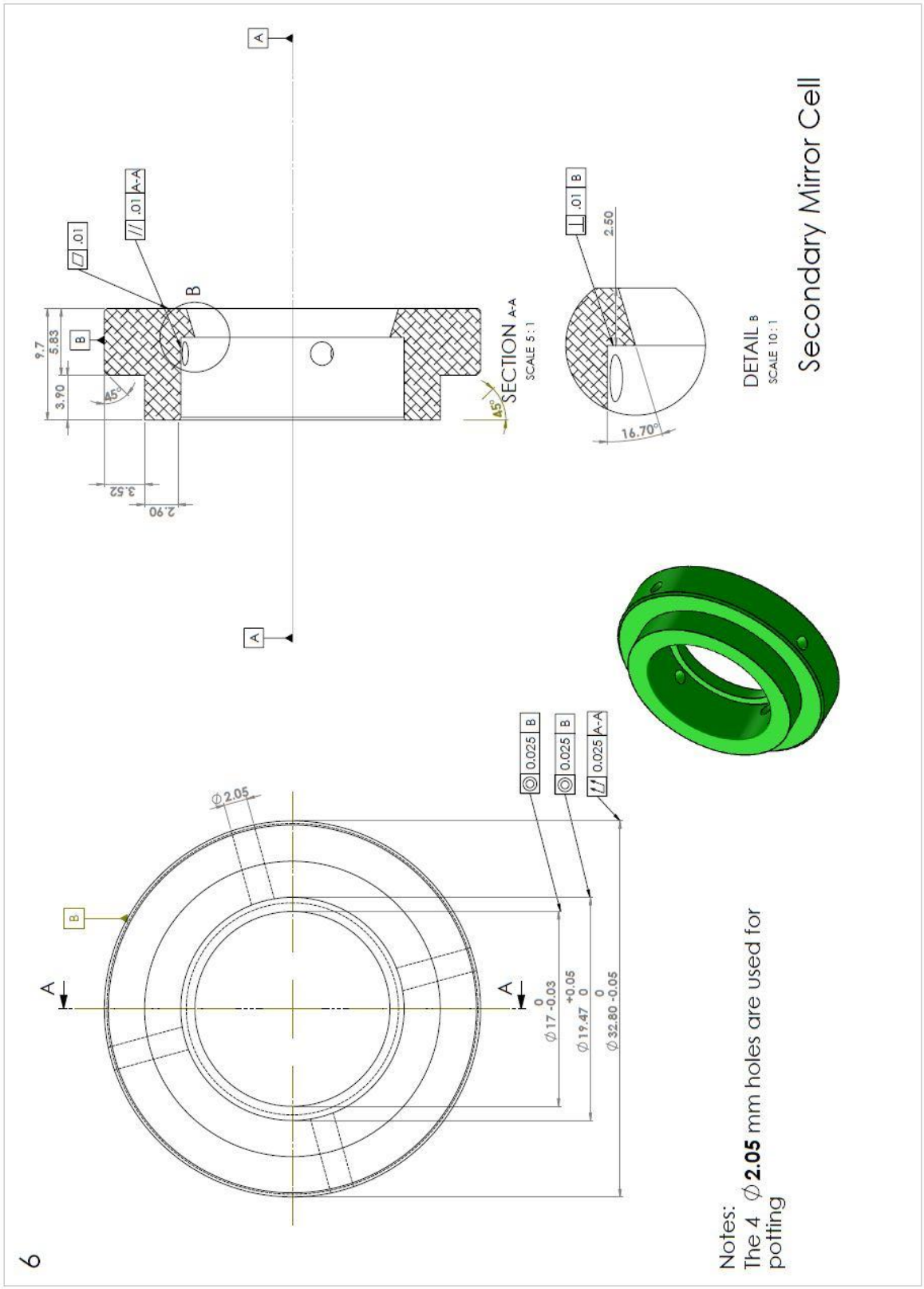

Secondary Spider Drawing

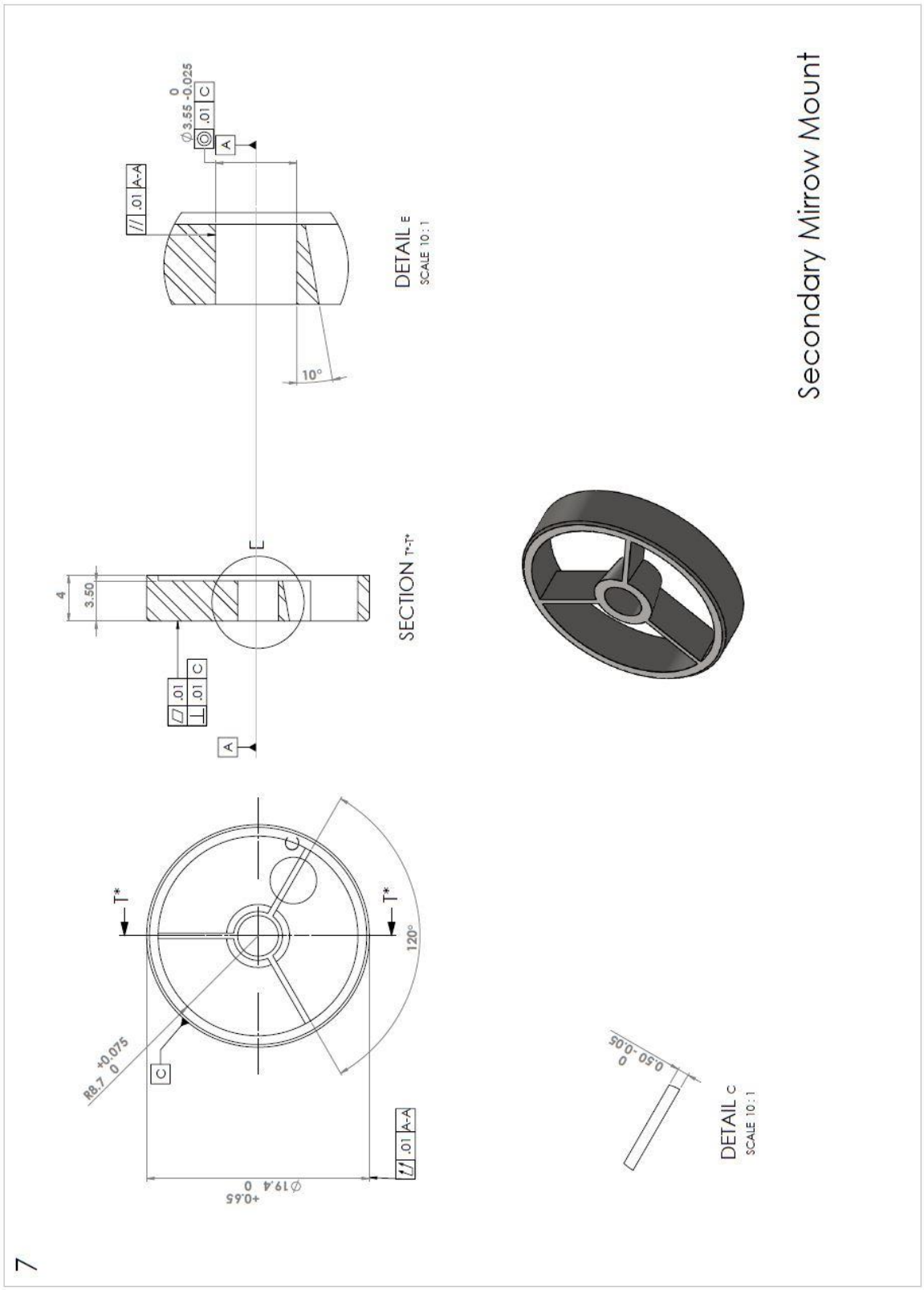

Secondary Mirror Drawing

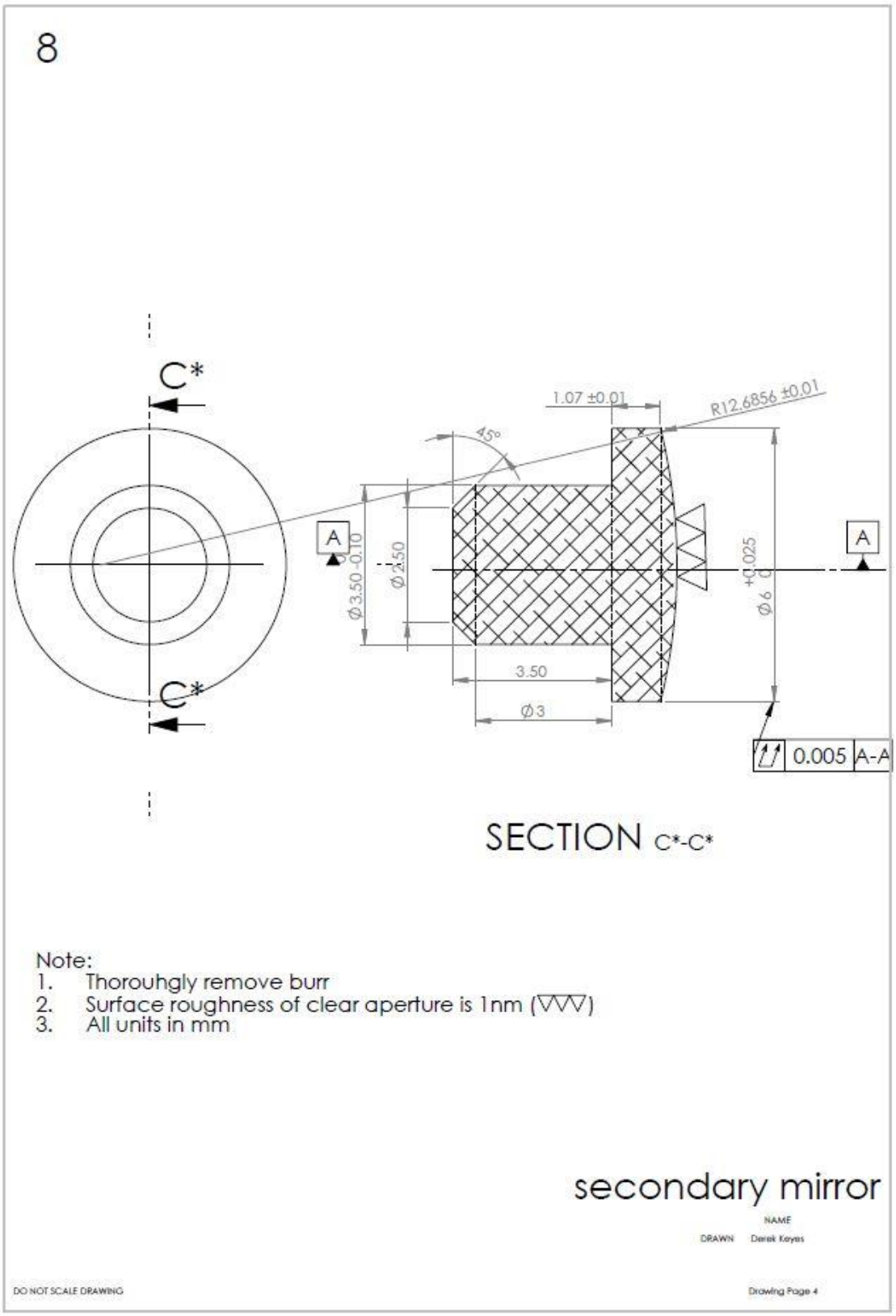

LiF Window Drawing

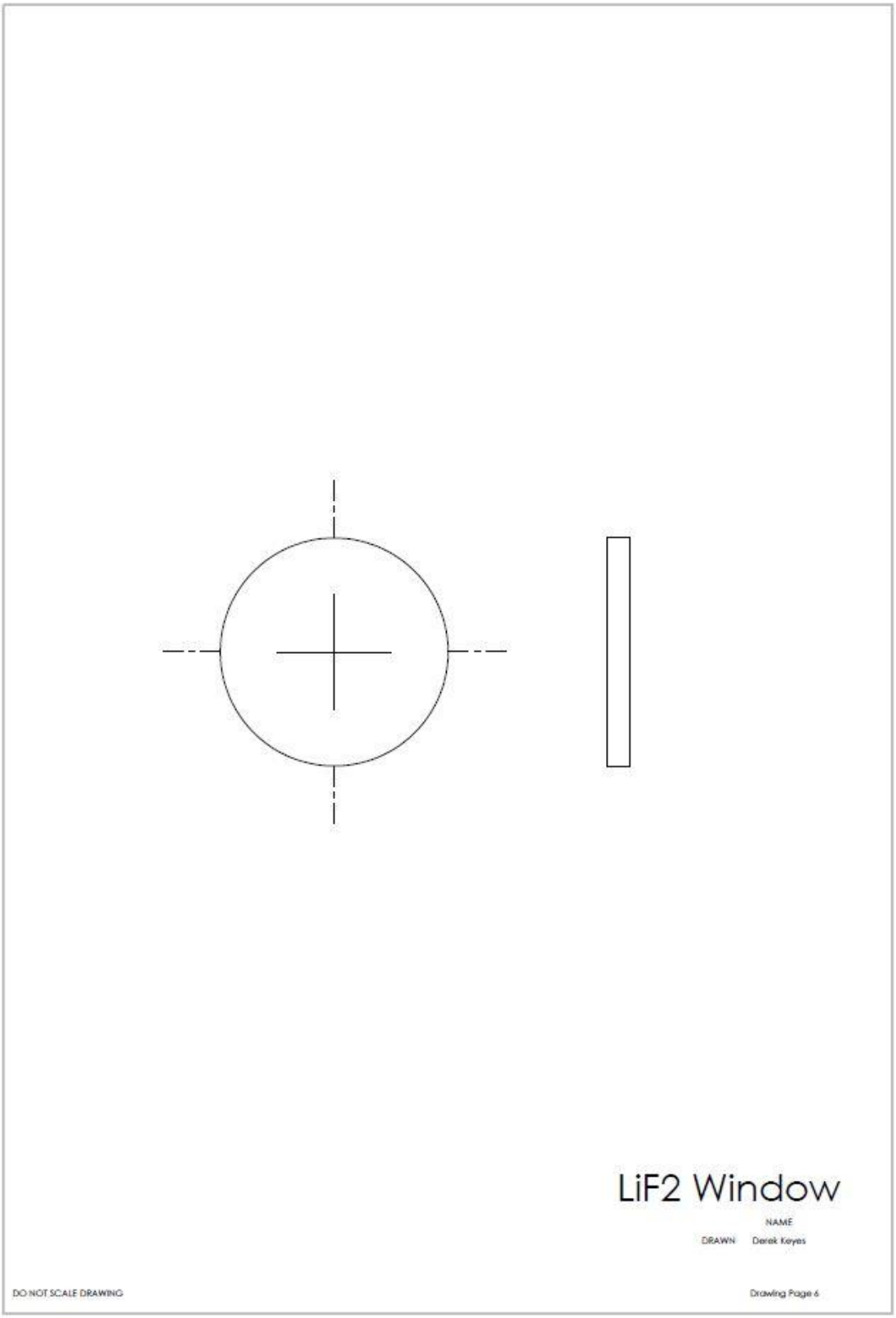

Shim Drawing

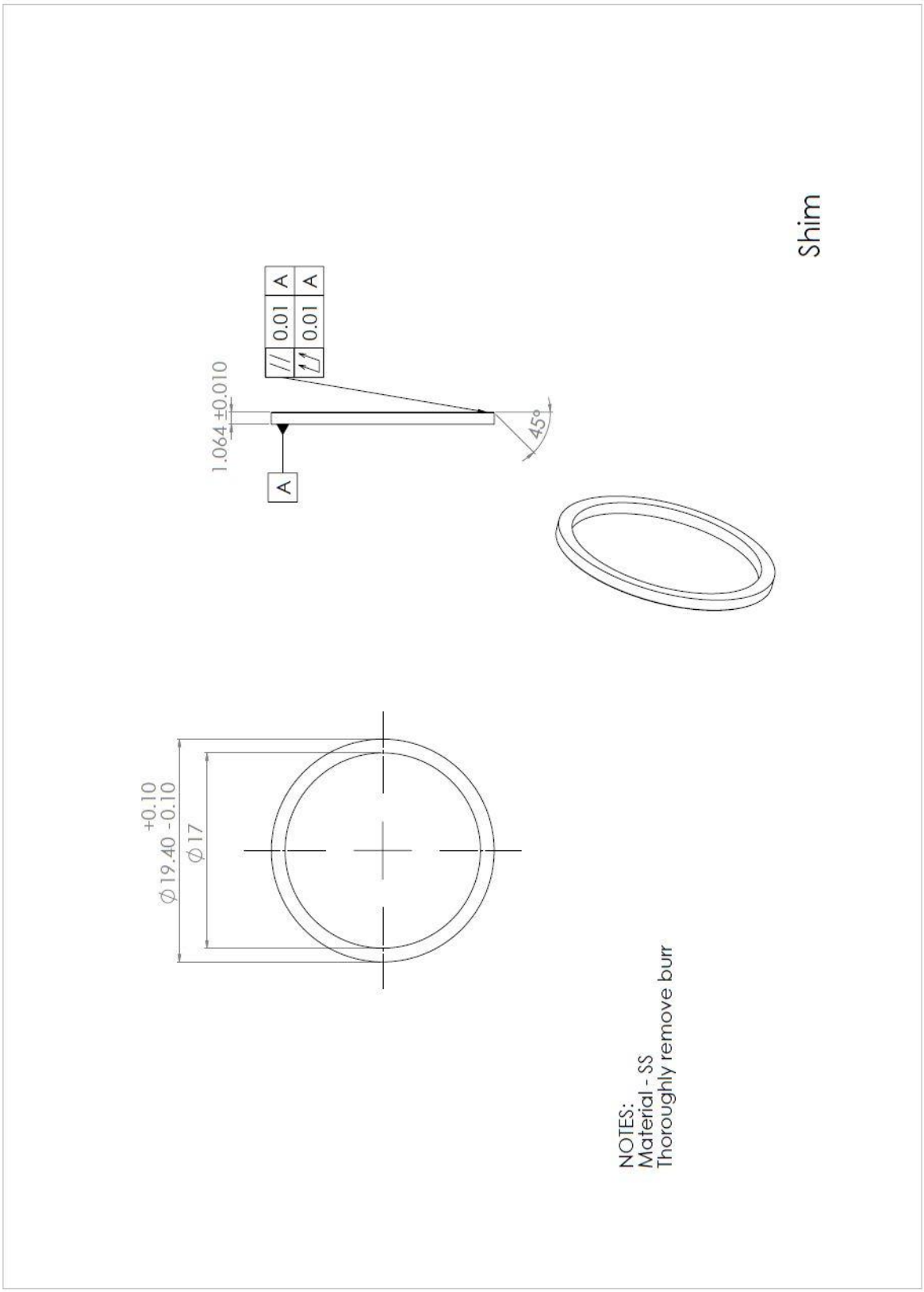

Retainer Ring Drawing

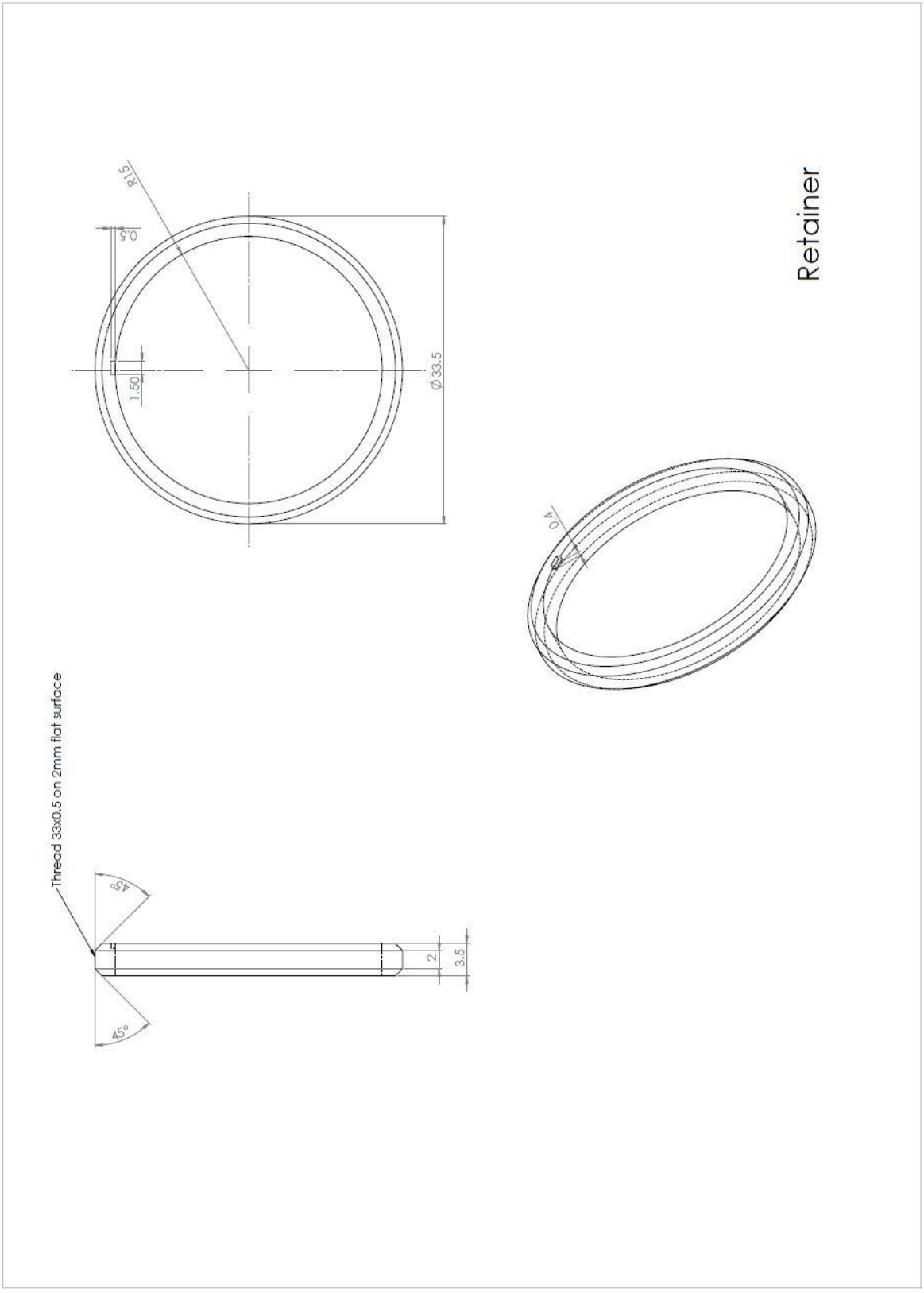

14. References

1. Jota, Thiago, et al. "Development of Optical Microscopy with a 121.6 nm Source." *Laser Science*. Optical Society of America, 2014.
2. Derek S. Keyes , et al." Optomechanical design and tolerance of a microscope objective at 121.6 nm ", Proc. SPIE 9575, Optical Manufacturing and Testing XI, 957506 (August 27, 2015); doi:10.1117/12.2188803
3. McCarthy, T. J., et al. "Non-thermal Doppler-broadened Lyman-α line shape in resonant dissociation of H2." *Journal of Physics B: Atomic, Molecular and Optical Physics* 38.16 (2005): 3043.
4. Esposito, Larry W., et al. "The Cassini ultraviolet imaging spectrograph investigation." *The Cassini-Huygens Mission*. Springer Netherlands, 2004. 299-361.
5. Esposito, Larry W., et al. "Ultraviolet imaging spectroscopy shows an active Saturnian system." *Science* 307.5713 (2005): 1251-1255.
6. Liberman, V., Rothschild, M., Murphy, P. G. & Palmacci, S. T. Prospects for photolithography at 121 nm. *J. Vac. Sci. Technol. B* 20, 2567–2573 (2002).
7. LaPorte, P., Subtil, J. L., Courbon, M., Bon, M. & Vincent, L. Vacuum-ultraviolet refractive index of LiF and MgF2 in the temperature range 80-300 K. *J. Opt. Soc. Am.* 73, 1062 (1983).
8. Chandrasekharan, V. & Damany, H. Anomalous dispersion of birefringence of sapphire and magnesium fluoride in the vacuum ultraviolet. *Appl. Opt.* 8, 671–675 (1969).

9. Schneider, E. G. Optical properties of lithium fluoride in the extreme ultraviolet. *Phys. Rev.* 49, 341 (1936).
10. Steinkopf, R., et al. "Metal mirrors with excellent figure and roughness."*Optical Systems Design*. International Society for Optics and Photonics, 2008.
11. R. Kingslake, *Lens Design Fundamentals*, Academic Press, p208 (1978).
12. Li, H. H. Refractive index of alkaline earth halides and its wavelength and temperature derivatives. *J. Phys. Chem. Ref. Data* 9, 161 (1980).
13. Horikawa, Y. *et al.* Design and fabrication of the Schwarzschild objective for soft x-ray microscopes. 1720, 0–8 (1992).
14. Yoder, Paul R. Mounting Optics in Optical Instruments. Bellingham: SPIE, 2008. Print.
15. Parks, R. & Kuhn, W. US Patent 20020054296 (2002).
16. Parks, R. E. & Kuhn, W. P. Optical alignment using the Point Source Microscope, *Proc. SPIE* 5877, 58770B–58770B–15 (2005).
17. Parks, R. E. Lens centering using the Point Source Microscope. *Proc. SPIE* 6676, 667603–667603–10 (2007).
18. Marshall, Jennifer L., et al. "Characterization of the reflectivity of various black materials." *SPIE Astronomical Telescopes+ Instrumentation*. International Society for Optics and Photonics, 2014.
19. Mimura, Takuo, Evelyn Anagnostou, and Paul E. Colarusso. *Thermal Radiation Absorptance and Vacuum Outgassing Characteristics of Several Metallic and Coated Surfaces*. No. NASA-TN-D-3234. NATIONAL AERONAUTICS AND SPACE ADMINISTRATION CLEVELAND OH LEWIS RESEARCH CENTER, 1966.

20. Persky, M. J. "Review of black surfaces for space-borne infrared systems."*Review of scientific instruments* 70.5 (1999): 2193-2217.
21. Kishkovich, Oleg P., et al. "Real-time methodologies for monitoring airborne molecular contamination in modern DUV photolithography facilities."*Microlithography'99*. International Society for Optics and Photonics, 1999.
22. "KOREA BASIC SCIENCE INSTITUE." KOREA BASIC SCIENCE INSTITUE. Web. 15 Mar. 2016.
23. Hasenauer, David. “Optical Design Tolerancing A Key to Product Cost Reduction.” Synopsys. 2015. July https://optics.synopsys.com/codev/pdfs/OpticalDesignTolerancing.pdf
24. Church, E. L. "Total integrated scatter measurements of surface roughness (A)." *Journal of the Optical Society of America (1917-1983)* 71 (1981): 1601.